MICROCOPY RESOLUTION TEST CHART
NATIONAL BUREAU OF STANDARDS-1963-A

AD-A182 594

INFRARED SENSOR DESIGN FOR

GEOSYNCHRONOUS ANTISATELLITE VEHICLES

THESIS

Jeffery G. Horne
Captain, USAF

AFIT/GSO/PH/84D-4

DEPARTMENT OF THE AIR FORCE

AIR UNIVERSITY

AIR FORCE INSTITUTE OF TECHNOLOGY

Wright-Patterson Air Force Base, Ohio

87   7 22 069

AFIT/GSO/PH/84D-4

INFRARED SENSOR DESIGN FOR

GEOSYNCHRONOUS ANTISATELLITE VEHICLES

THESIS

Jeffery G. Horne
Captain, USAF

AFIT/GSO/PH/84D-4
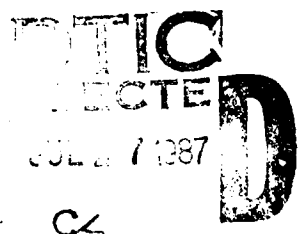
Approved for public release; distribution unlimited

INFRARED SENSOR DESIGN FOR GEOSYNCHRONOUS

ANTISATELLITE VEHICLES

THESIS

Presented to the Faculty of the School of Engineering

of the Air Force Institute of Technology

Air University

In Partial Fulfillment of the

Requirements for the Degree of

Master of Science in Space Operations

Jeffery G. Horne, B.A., M.S

Captain, USAF

December 1984

Acknowledgments

In performing the investigation, analysis and writing this thesis, I have had a great deal of help from others. I am much indebted to my faculty advisor, Major James J. Lange, for his ideas, suggestions, directions, and corrections. I would also like to thank my wife Valerie, for her much needed support and assistance.

Contents

iv

List of Figures

List of Tables

Abstract

The maximum distance from which a possible antisatellite sensor can reliably detect its target was investigated based upon the celestial background radiation at a wavelength of 11 microns. A sensor design was postulated and assessed with various background conditions.

The analysis was first conducted using the Walker Sky Model to estimate the amount of infrared background radiance from stellar sources. Then this estimate was compared with cataloged observations for the Air Force Geophysics Lab catalog and preliminary data from the Infrared Astronomical Telescope. In addition, the amount of infrared radiation from asteroids and zodiacal light particles was also considered.

The results of the analysis indicates that for a sensor using a single detector, a spinning reticle, and optics 20 centimeters in diameter, the maximum range that a one square meter target can be detected reliably is between 1300 and 2300 kilometers. However, more investigations into the infrared stellar and zodiacal light background are needed as the currently available data is incomplete.

INFRARED SENSOR DESIGN FOR GEOSYNCHRONOUS
ANTISATELLITE VEHICLES

I. Introduction

In order for an antisatellite (ASAT) vehicle to be
effective against a satellite target, it must first detect
the target. This means detecting the target at a large
enough distance away to allow the ASAT to maneuver into an
orbit that will result in interception. The United States
has been developing an ASAT that can detect low altitude
satellite targets at a range of a few hundred kilometers.
If a similar ASAT is to be effective against higher
orbiting targets, the ASAT sensor must detect these targets
at a much greater range.

The current United States ASAT uses an infrared sensor
to acquire its potential targets (5). The use of an
infrared sensor allows the sensor to acquire targets
without the need for reflected sunlight since any satellite
emits infrared radiation. Most satellites are at a
temperature of 275 to 300 degrees Kelvin. The wavelength
where the maximum energy output occurs for these
temperatures occurs around ten microns.

Unfortunately, satellites are not the only celestial
objects radiating energy at a wavelength of ten microns.

Energy sources include planets, asteroids, comets, the earth itself, interplanetary and interstellar dust and gas, as well as all the stars in our Milky Way galaxy. It is the vast number of stars in the galaxy and the interplanetary dust within the solar system that causes the greatest source of background radiation at ten microns.

Detecting a target satellite against such a background is made more difficult as the target is moved further and further from the sensor. To complicate matters even more, the celestial infrared background is by no means uniform. The amount of background radiation can vary by more than two orders of magnitude. The majority of stars are located close to the galactic equator, with fewer stars at higher latitudes.

Two problems arise. What kind of infrared sensor is required to detect target satellites against such a background? What is the maximum distance the sensor can be from the target and still expect to acquire its target? This distance will depend upon the complexity of the infrared sensor, the scan time, and the area of the sky the target is located in.

This thesis will determine values for the infrared background and will estimate the maximum range a sample sensor can be from a target, and still detect it reliably.

Chapter 2 of this thesis will present background material on celestial infrared radiation and infrared

2

sensors used in spacecraft.

Chapter 3 will discuss the two sources of infrared sky data and introduce the Walker Sky Model to determine the infrared radiance from different regions of the sky.

Chapter 4 will present the parameters of sensor design and determine the maximum detection ranges for a sample sensor.

Chapter 5 will present analysis of the Walker Sky Model, and discuss its accuracy.

Chapter 6 will present needed additions to the Walker sky model and revised maximum sensor ranges.

Chapter 7 will present conclusions drawn from the analysis and make recommendations for further studies.

II. Background

The backdrop for this problem lies in two sections. First, what data exists on the infrared celestial background? Second, what infrared sensors have been used in the past to detect exoatmospheric objects?

Infrared Sky Surveys

Two surveys of infrared celestial radiation around the wavelength of ten microns were made during the 1970's and one survey was made in the current decade. The first one was the Celestial Mapping Program (CMP) by Grish and Lynch (23:2-8). The second survey was the Air Force Geophysical Laboratory Four Color Sky Survey by Price and Walker (27). The Air Force Geophysical Lab (AFGL) survey has better positional accuracy than the CMP, but the AFGL survey has gaps in its coverage.

The most recent survey of the infrared celestial background was the Infrared Astronomical Satellite (IRAS) program. The IRAS survey results contain more than two hundred thousand sources at wavelengths greater than twelve microns. (2). Unfortunately, only a small portion of the IRAS data catalog is available. This data is part of the IRAS "Minisurvey" that was conducted before the all-sky survey was made. This minisurvey consists of a region approximately 300 square degrees in size. This minisurvey

was made to test the IRAS components before the main survey began. The data from this minisurvey includes observations of sources with irradiances values on the order of 1.0E-18 $W-cm^{-2}-um^{-1}$ or larger (29).

Several classes of objects are the most significant contributors to the infrared sky background at ten microns. These include late type K and M stars, stars deeply reddened by absorption from interstellar dust, H-II regions (pronounced H-two) (23:2-8), and the zodiacal light particles (19:458). H-II regions are interstellar clouds of ionized hydrogen gas. The zodiacal light is reflected sunlight from interplanetary dust within our solar system (1:253). Analysis by Price and Walker shows that over half the sources listed in the AFGL catalog are from either H-II regions or stars reddened by interstellar dust. The H-II regions in the sun's neighborhood have considerable angular size, ranging from several arc minutes to several degrees across. Most of the stellar and H-II sources are confined within five degrees of the galactic plane. Walker and Price also state that many extended, low intensity celestial objects are not included in the AFGL catalog because of their low surface radiance (23:2-8).

The measurement of emission from the interplanetary dust that causes the zodiacal light has been more difficult because of the large angular extent of the emission source. Briotta, Piper, and Houck made observations in the eight to

5

twelve micron range, but their observations were seriously contaminated with radiation from the earth (24:771). Observations have also been made by the AFGL, but the data is measured relative to the non-ecliptic background, and is not in terms of absolute radiances (23:2-10).

In addition to the three classes of ten micron radiation mentioned above, asteroids also present a possible background source. The total number of asteroids in the solar system is unknown, but is estimated to be far in excess of the 3000 for which orbits have been calculated. From observations at eleven microns, asteroids temperatures have been estimated to be between 200 to 260 degrees Kelvin. This is the range in which earth orbiting satellites would be found (23:2-11). Murdock (21) made a study to predict the number of asteroids visible an any one time. The asteroids are concentrated within seven degrees of the ecliptic plane. The density of asteroids along the ecliptic plane may be several per square degree and contribute $1.0E-19$ $W-cm^{-2}-um^{-1}$ to the background irradiance at eleven microns (23:2-11).

A recent work by Grasdalen et al (9:413) tried to correlate AFGL sky survey sources to ground based observations. The effort was to isolate that portion of the AFGL sky survey that included only stellar objects. Another objective of this study was to estimate the type and number of sources the Infrared Astronomical Satellite

6

(IRAS) would be likely to encounter. The study estimated that IRAS would see about 100,000 more sources than the AFGL survey, but the mixture of sources would not be substantially different than those seen by the AFGL survey.

As mentioned previously, the most recent work in the measurement of the celestial background between eight and fifteen microns was conducted by IRAS. Preliminary analysis of data indicates an additional ring of dust particles further from the sun than the ring that causes the zodiacal light. The temperature of the dust is estimated to be between 165 and 200 degrees Kelvin (28:5). Some of data gathered from earlier investigations was confirmed by IRAS. This included the contribution to the background from very large emission sources (H-II regions) located within the galactic plane, and the fact that the galactic nucleus was shown to be an especially strong emitter (2:122). However, the IRAS measured zodiacal emission measurements exceeds previously published measurements at eleven microns (11:617). The interpretation of the data indicates that the emission stems from optically thin clouds of dust which are not at a single temperature.

Infrared Space Sensors

Various infrared space sensors have been designed or developed for detecting satellites over the past decade. These can be divided into two relevant categories: ground

7

based and space based.

Work in this area for a deep space tracking network was accomplished in the early 1970's. This work was done before the decision was made to use a visual sensor for the Ground-Based Deep Space Surveillance System (GEODSS). Proposals included an airborne Long Wave Infrared (LWIR) sensor deployed on aircraft above thirty thousand feet (34). NASA's Kuiper airborne infrared observatory has a C-141 and uses a similar approach for astronomical research. The most successful ground based development in this area is the Maui Optical Tracking and Identification Facility (MOTIF) on Mount Haleakala in Hawaii. This sensor continues to do active research and spacetrack augmentation.

The MOTIF sensor consists of a 1.2 meter Cassegrain telescope with an LWIR radiometer attached. The sensor array consists of 25 germanium-cadmium detectors cooled to 13 degrees Kelvin. The infrared range is from 3 to 22 microns in seven different bands. The field of view for the sensor is 80 arc seconds.

The MOTIF sensor has been used to determine LWIR signatures of foreign satellites as well as investigations into the LWIR radiance of the atmosphere. The objectives of the satellite infrared signature program are to obtain both passive and active infrared signatures in the 8 to 13 and 17 to 21 micron bands. This program tries to gather

8

sufficient data on specific satellites to allow the prediction of signatures for satellites that cannot or have not been observed (30).

In the 1974-5 timeframe, several studies were commissioned to design a space based satellite tracking satellite. Studies were made by Philco Ford Corporation, Lockheed Missiles and Space Corporation, and Rockwell International (15).

After the early studies were completed, an experimental satellite was contracted for in order to increase the data base necessary to accurately design an LWIR space surveillance system satellite. This experimental satellite was known as the Space Infrared Experiment (SIRE). The satellite was originally scheduled to be launched in 1981, but the project was delayed and eventually abandoned because of large anticipated costs (33). However, the technology developed for this program may be used on a future space surveillance system (35). The infrared sources the satellite was to investigate included earth limb radiance, zodiacal light, stellar radiation, and asteroids, as well as satellites. The satellite was designed to determine which spectral band in the infrared gave the best possibility of detecting a target satellite. Also, this satellite would have provided a test of the optics and two dimensional detector array (18).

9

The SIRE satellite was to be a cryogen cooled sensor covering the 7 to 23 micron range in five separate bands. It was to use a three mirror anastigmat optical configuration with a collecting area of 435 square centimeters. This arrangement would allow for detection and tracking of objects in both low earth, and geosynchronous orbits (18).

Several spacecraft have used long wavelength infrared sensors as part of their instrumentation. These spacecraft include Landsat D, the Defense Meteorological Satellite (DMSP), the United States ASAT test project, and the Infrared Astronomical Satellite (IRAS) (11).

The IRAS sensor was used to conduct a survey of the entire sky from an altitude of 900 kilometers. This sensor conducted observations in four infrared bands: 12, 25, 60, and 100 microns. The detectors for these bands were silicon-arsenide, silicon-tin, germanium-gallium, and germanium-gallium respectively. The entire sensor consisted of a telescope 0.57 meters in diameter with a five meter focal length. The focal plane array with the detectors was cooled to less than three degrees Kelvin. The two mirror beryllium optical system (Ritchey-Chretien) was cooled to less than ten degrees Kelvin by liquid helium.

The focal plane assembly was constructed so that every infrared source crossing the 60 arc minute field of view

10

could be seen by at least two detectors in each wavelength band. The position of each source seen by the 16 detectors in the 12 micron band lies in an uncertainty ellipse approximately 45 x 9 arc seconds. Each detector was covered by a field lens and a filter giving a mean in-band transmission of 83 percent for the 12 micron band. The system in-band noise equivalent flux density (NEFD) was on the order of 1.0E-19 W-cm^{-2} averaged across the spectral bandpass. (20:69).

III. The Infrared Sky

There are two major catalogs of infrared stars. One is from the Air Force Geophysics Lab Sky Survey. This data catalog was compiled from nine rocket flights between 1971 and 1974. The catalog was published in 1976. At eleven microns, 90 percent of the sky was surveyed at least once and about 60 per cent of the sky was mapped two or more times (27:9). The AFGL catalog lists 1151 sources at eleven microns. Through data reduction and spurious source elimination, the AFGL considers the catalog complete down to an irradiance level of 2.2E-16 $W-cm^{-2}-um^{-1}$ at eleven microns. The catalog does list some sources as faint as 1.2E-16 $W-cm^{-2}-um^{-1}$ (27:14). These 1151 sources are not spread out evenly across the sky, but the majority are within plus or minus 20 degrees of the galactic plane.

The second catalog is the NASA Catalog of Infrared Observations. This catalog is a listing of all the astronomical observations in the infrared between 1 and 1000 microns, which were published in the scientific literature from 1965 through 1982. This catalog contains over 85,000 individual observations of about 10,000 different infrared sources. The catalog was published in May 1984 (8:1). This catalog contains the data from the AFGL catalog, and additional data. The NASA catalog has objects listed as faint as 1.2E-18 $W-cm^{-2}-um^{-1}$, but these

12

entries are sporadic and far from complete.

The two major infrared source catalogs only contain reliably complete data as faint as 1.0E-16 $W\text{-}cm^{-2}\text{-}um^{-1}$. Since spacecraft target intensities can be as faint as 1.0E-18 $W\text{-}cm^{-2}\text{-}um^{-1}$ (10:61), a source of data for stars at this irradiance level and lower must be found. IRAS data includes stars this faint, but its entire data catalog is unavailable at present.

The Walker Sky Model

Walker has developed a model for estimating the density and hence irradiance levels for infrared sources within the galaxy (36:3-28). This model estimates the number of sources observed at irradiance levels from 1.0E-14 to 1.0E-20 $W\text{-}cm^{-2}\text{-}um^{-1}$ at various galactic latitudes and longitudes.

The model represents the galaxy as a planar disk with a dense central bulge. The center of the galaxy is at a distance R = 1.0E4 parsecs (1 parsec = 3.09E18 cm) from the Sun. Galactic coordinates are l for longitude, measured from the Sun galactic center line, and b for latitude, measured from the galactic disk. The galaxy is shown graphically in figure 1.

The model of infrared sources is considered to be a Gaussian distribution of the form A exp - $(X/\sigma)^2$ where X is the distance above the galactic plane and σ is the

13
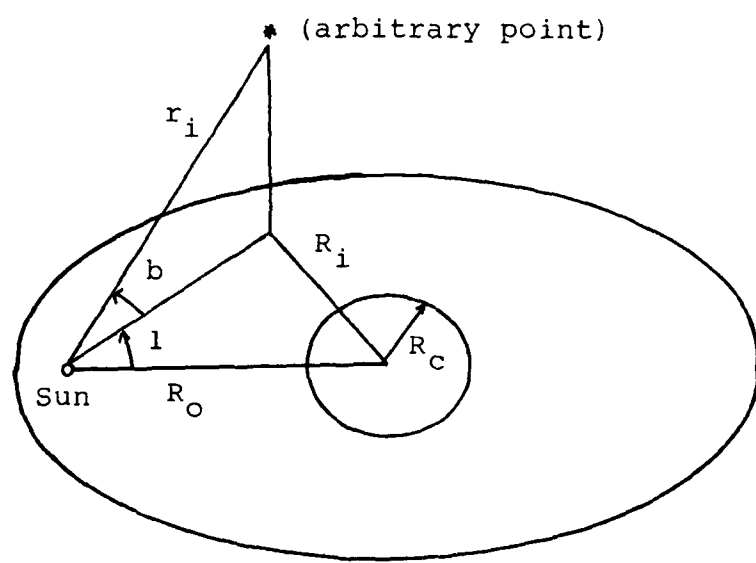
Figure 1. Graphic Model of the Galaxy

standard deviation of the galactic distribution of
infrared sources in terms of perpendicular distance from
the galactic plane (10). Several classes of objects
contribute to the infrared source model. These are dwarf
stars (mass less than 10 solar masses, 1 solar mass =
1.991E33 grams), giant stars (mass less than 50 solar
masses), supergiant stars (mass greater than 50 solar
masses), and HII regions (1). The dispersions, σ_i , normal
to the galactic plane are 160 parsecs for dwarf stars, 450
parsecs for giant stars, 100 parsecs for supergiant stars,
and 100 parsecs for HII regions.

The nucleus of the galaxy contains more sources per
volume than does the rest of the galaxy. The Gaussian
distribution is modified by the factor,

$$\frac{R_C^2}{R_C^2 + R_C^2}$$

where R_C is the radius of the galactic nucleus = 9.27E21
cm, and R_i is the distance (shown in figure 1) in the
galactic plane from the galactic center to some arbitrary
point.

This model is represented by a single, though
complex equation:

$$N = k \sum_{i=1}^{M} n_i \, I_{\lambda,i}^{3/2} \int_{E_{\lambda(i,M)}}^{\infty} \left(\frac{R_c^2}{R_c^2 + R_i^2} \right) E_\lambda^{-5/2} \, exp\left[\frac{-I_{\lambda,i}}{E_\lambda} \left(\frac{\sin b}{\sigma_i^2} \right)^2 \right] d E_\lambda$$

15

where

N = the number of infrared sources per square degree in some arbitrary direction along by r_i (specified by angles b,l), producing irradiance at the observer which is greater than $E_{\lambda_{lim}}$,

$E_{\lambda_{lim}}$ = the limiting spectral irradiance in $W\text{-}cm^{-2}\text{-}um^{-1}$,

$I_{\lambda,i} = a_i \lambda^{c_i}$, the mean spectral radiant intensity of the ith class of celestial objects in watts/ster,

n_i = the mean space density of the ith class of sources in numbers/cm^3,

l = galactic longitude in degrees east from a line between the observer and galactic center,

b = galactic latitude in degrees above or below the plane of the galaxy as seen from the observer's location,

R_o = the distance from the Sun (and observer) to the galactic center = 3.09E22 cm,

R_c = the radius of the galactic nucleus = 9.27E21 cm,

σ_i = the dispersion of the ith class normal to the galactic plane in cm,

λ = the wavelength,

$$R_i^2 = I_{\lambda,i} E_\lambda^{-1} \cos(b)^2 + R_o^2 - 2R_o I_{\lambda,i}^{\frac{1}{2}} E_\lambda^{-\frac{1}{2}} \cos(b) \cos(l) + I_{\lambda,i} E_\lambda^{-1} \cos(b),$$

a_i, c_i = constants observationally determined which describe the intensity of the generic member of the ith class, and

16

$$k = 1.52E-4 \quad ster-deg^{-2}.$$

The values for σ_i, n_i, a_i, and c_i for the model are derived from sky survey and other astronomical data (10:121) and are given in table I. The irradiances caused by emission nebulae (H-II) have been included with the supergiants because they have similar space distributions.

The value for R_i is determined using the law of cosines (see figure 1)

$$R_i^2 = R_o^2 + (r_i \cos(b))^2 - 2R_o(r_i \cos(b)) \cos(1),$$

and the point source intensity-irradiation relation

$$E_\lambda = I_{\lambda,i} / r_i^2 .$$

The equation for the model, while not obvious, is a best fit to the AFGL and other data (10), and does check out to be dimensionally correct. A discussion of its construction is found in Appendix D.

Table I

Constants for the Galactic Source Model

Class	σ_i	n_i	a_i	c_i
Dwarfs	4.94E+20	2.63E-56	2.77E+24	-3.693
Giants	1.39E+21	9.46E-60	1.07E+28	-1.915
H II regions & supergiants	3.09E+20	8.07E-62	1.09E+29	-1.108
units	cm	stars-cm^{-3}	W-sr^{-1}-um^{-1}	--

17

The model will yield the number of sources for any particular direction defined by b and l, and for a particular wavelength defined by λ. To evaluate the integral for each wavelength region, the interval of integration was broken into three latitude ranges and numerical integration was done by means of 16-point Legendre-Gauss quadrature. This was done by Walker (36:3-30) and Greenebaum (10:127).

The results the integration for eleven microns are shown in table II (10:134). Since the galaxy is considered to be symmetric, the values for negative latitudes will be the same as those for positive latitudes. The same can be said for longitude between 0 and 180 degrees, and those between 180 and 360 degrees.

This table lists the number of infrared sources per square degree at a wavelength of eleven microns for selected areas of the galaxy. The spectral irradiance is in Watts-cm^{-2}-um^{-1}. Each item in the body of the table is the sum of all sources to the limit of the spectral irradiance for that row in the table. For example, for galactic latitude 0 degrees, longitude 0 degrees there are 9400 infrared sources at a spectral irradiance level of 1.0E-18 Watts-cm^{-2}-um^{-1} and brighter.

To find the total radiance per square degree for any particular area, the contribution of each spectral irradiance level must be calculated. Since each entry in

18

TABLE II

NUMBER OF SOURCES PER SQUARE DEGREE AT 11.0 MICRONS

SPECTRAL IRRADIANCE	GALACTIC LATITUDE (DEGREES)									GALACTIC LONGITUDE
	0	2	5	10	20	30	45	60	90	
1.0E-14	5.6E-4	5.6E-4	5.4E-4	5.0E-4	3.6E-4	2.5E-4	1.6E-4	1.3E-4	1.2E-4	0
1.0E-14	5.5E-4	5.5E-4	5.4E-4	4.9E-4	3.6E-4	2.5E-4	1.6E-4	1.3E-4	1.2E-4	45
1.0E-14	5.4E-4	5.4E-4	5.2E-4	4.8E-4	3.5E-4	2.5E-4	1.6E-4	1.3E-4	1.2E-4	90
1.0E-14	5.2E-4	5.2E-4	5.1E-4	4.7E-4	3.5E-4	2.4E-4	1.6E-4	1.3E-4	1.2E-4	180
1.0E-15	1.9E-2	1.8E-2	1.4E-2	7.4E-3	3.6E-3	3.1E-3	2.9E-3	2.8E-3	2.8E-3	0
1.0E-15	1.8E-2	1.8E-2	1.4E-2	7.3E-3	3.5E-3	3.0E-3	2.9E-3	2.8E-3	2.8E-3	45
1.0E-15	1.7E-2	1.6E-2	1.3E-2	6.9E-3	3.5E-3	3.0E-3	2.9E-3	2.8E-3	2.8E-3	90
1.0E-15	1.5E-2	1.5E-2	1.2E-2	6.5E-3	3.4E-3	3.0E-3	2.8E-3	2.8E-3	2.8E-3	180
1.0E-16	7.9E-1	4.8E-1	1.4E-1	9.8E-2	9.1E-2	8.6E-2	7.8E-2	7.2E-2	6.5E-2	0
1.0E-16	6.8E-1	4.3E-1	1.4E-1	9.7E-2	8.9E-2	8.5E-2	7.8E-2	7.1E-2	6.5E-2	45
1.0E-16	5.2E-1	3.4E-1	1.3E-1	9.4E-2	8.7E-2	8.2E-2	7.6E-2	7.0E-2	6.5E-2	90
1.0E-16	4.0E-1	2.7E-1	1.2E-1	8.9E-2	8.3E-2	7.9E-2	7.3E-2	6.8E-2	6.5E-2	180
1.0E-17	9.3E1	4.6E0	3.3E0	3.0E0	2.2E0	1.5E0	7.6E-1	4.4E-1	2.8E-1	0
1.0E-17	2.8E1	4.0E0	3.1E0	2.8E0	2.1E0	1.4E0	7.4E-1	4.4E-1	2.8E-1	45
1.0E-17	1.3E1	3.4E0	2.8E0	2.5E0	1.9E0	1.3E0	6.9E-1	4.2E-1	2.8E-1	90
1.0E-17	8.0E0	2.8E0	2.4E0	2.2E0	1.7E0	1.3E0	6.4E-1	4.0E-1	2.8E-1	180
1.0E-18	9.4E2	1.5E2	1.2E2	5.7E1	9.3E0	2.7E0	8.8E-1	4.6E-1	2.9E-1	0
1.0E-18	3.6E2	1.2E2	9.5E1	4.7E1	8.4E0	2.5E0	8.6E-1	4.6E-1	2.9E-1	45
1.0E-18	1.9E2	8.1E1	6.6E1	3.4E1	6.9E0	2.3E0	8.0E-1	4.4E-1	2.9E-1	90
1.0E-18	1.2E2	5.7E1	4.7E1	2.5E1	5.6E0	1.9E0	7.3E-1	4.2E-1	2.9E-1	180
1.0E-19	2.5E4	1.5E4	2.0E3	1.1E2	9.5E0	2.8E0	9.6E-1	5.5E-1	3.8E-1	0
1.0E-19	5.6E3	3.3E3	6.9E2	7.7E1	8.6E0	2.6E0	9.4E-1	5.4E-1	3.8E-1	45
1.0E-19	2.3E3	1.3E3	3.2E2	5.0E1	7.0E0	2.3E0	8.6E-1	5.3E-1	3.8E-1	90
1.0E-19	1.3E3	6.9E2	1.9E2	3.5E1	5.7E0	2.0E0	8.1E-1	5.0E-1	3.8E-1	180
1.0E-20	1.0E5	3.1E4	2.1E3	1.1E2	1.1E1	4.4E0	2.6E0	2.1E0	1.9E0	0
1.0E-20	3.6E4	7.0E3	7.1E2	7.9E1	1.0E1	4.3E0	2.6E0	2.1E0	1.9E0	45
1.0E-20	1.7E4	2.6E3	3.3E2	5.2E1	8.7E0	4.0E0	2.5E0	2.1E0	1.9E0	90
1.0E-20	1.0E4	1.4E3	1.9E2	3.6E1	7.3E0	3.7E0	2.4E0	2.1E0	1.9E0	180

Irradiance is in Watts-cm^{-2}-um^{-1}

the table represents a sum of all the sources to that level of brightness, the sources brighter than that particular level must be subtracted in order to obtain the irradiance from that level only. That is, to find the number of sources only at an irradiance range of 1.0E-15 Watts-cm^{-2}-um^{-1}, to 10E-15 the number of sources at 1.0E-14 must be subtracted from the number for 1.0E-15 listed in the table. The number of sources at a particular irradiance range times the average irradiance of that range will give that ranges's contribution to the total radiance from a galactic region. The sum of the irradiance level contributions gives the total radiance for that area.

For example, to find the total radiance from a region around galactic latitude 10 degrees, longitude 45 degrees, the total number of individual components must first be calculated, as shown below.

From table II,

Irradiance E_λ W-cm -um	Number of Sources with $E_\lambda > E_{\lambda_o}$
1.0E-14	4.9E-4
1.0E-15	7.3E-3
1.0E-16	9.7E-2
1.0E-17	2.8E0
1.0E-18	4.7E1
1.0E-19	7.7E1
1.0E-20	7.9E1

Irradiance Ranges of E_{λ_o}	Number of Sources in Irradiance Range		
> 1.0E-14	4.9E-4 - 0 =		4.90E-4
1.0E-14 to 1.0E-15	7.3E-3 - 4.9E-4 =		6.81E-3
1.0E-15 to 1.0E-16	9.7E-2 - 7.3E-3 =		8.97E-2
1.0E-16 to 1.0E-17	2.8E0 - 9.7E-2 =		2.70E0
1.0E-17 to 1.0E-18	4.7E1 - 2.8E0 =		4.42E1
1.0E-18 to 1.0E-19	7.7E1 - 4.7E1 =		3.00E1
1.0E-19 to 1.0E-20	7.9E1 - 7.7E1 =		2.00E0

Next, the individual numbers must be multiplied by the irradiance levels to find the contribution from that irradiance level. That is:

Number	Irradiance $W\text{-}cm^{-2}\text{-}um^{-1}$	Contribution	
(4.90E-4)	x (1.0E-14)	=	4.90E-18
(6.81E-3)	x (1.0E-15)	=	6.81E-18
(8.97E-2)	x (1.0E-16)	=	8.97E-18
(2.70E0)	x (1.0E-17)	=	2.70E-17
(4.42E1)	x (1.0E-18)	=	4.42E-17
(3.00E1)	x (1.0E-19)	=	3.00E-18
(2.00E0)	x (1.0E-20)	=	2.00E-20

The irradiance at the bottom of each range is chosen as the average value for the range because the number of sources is greatest at lower irradiances.

21

Since table II gives the number of sources per square degree in each irradiance range, summing the radiance contribution from each irradiance range will give the total radiance expected from a particular 1 degree by 1 degree region of the sky.

Summing the individual contributions calculated above gives the total radiance for the 1 degree by 1 degree region of the sky around latitude 10 degrees, longitude 45 degrees. It is 9.49E-17 Watts-cm^{-2}-um^{-1}-deg^{-2}, or 6.245E-13 Watts-cm^{-2}-um^{-1}-ster^{-1}.

The radiance calculations for each sky area of table II are shown in table III. Table III shows total radiance in Watts-cm^{-2}-um^{-1}-ster^{-1} for the galactic positions shown. The radiances calculated in this table are in general agreement with those found in the Infrared Handbook (36:3-32). From this table a contour map can be created showing the expected radiances as a function of galactic position. This is shown in figure 2.

TABLE III

TOTAL RADIANCE IN WATTS-CM^{-2}-UM^{-1}-$STER^{-1}$

GALACTIC LATITUDE	GALACTIC LONGITUDE			
	0	45	90	180
0	3.31E-11	1.00E-11	4.81E-12	2.97E-12
2	1.25E-11	3.76E-12	1.95E-12	1.28E-12
5	2.43E-12	1.40E-12	9.52E-13	7.18E-13
10	7.19E-13	6.25E-13	5.07E-13	4.20E-13
20	2.88E-13	2.75E-13	2.51E-13	2.28E-13
30	1.91E-13	1.82E-13	1.73E-13	1.62E-13
45	1.24E-13	1.22E-13	1.18E-13	1.12E-13
60	9.61E-14	9.55E-14	9.36E-14	9.11E-14
90	8.08E-14	8.08E-14	8.08E-14	8.08E-14

All Units Watts–cm^{-2}–um^{-1}–ster^{-1}

1.0E-13

5.0E-13

1.0E-12

5.0E-12

5.0E-13

1.0E-13

1.0E-11
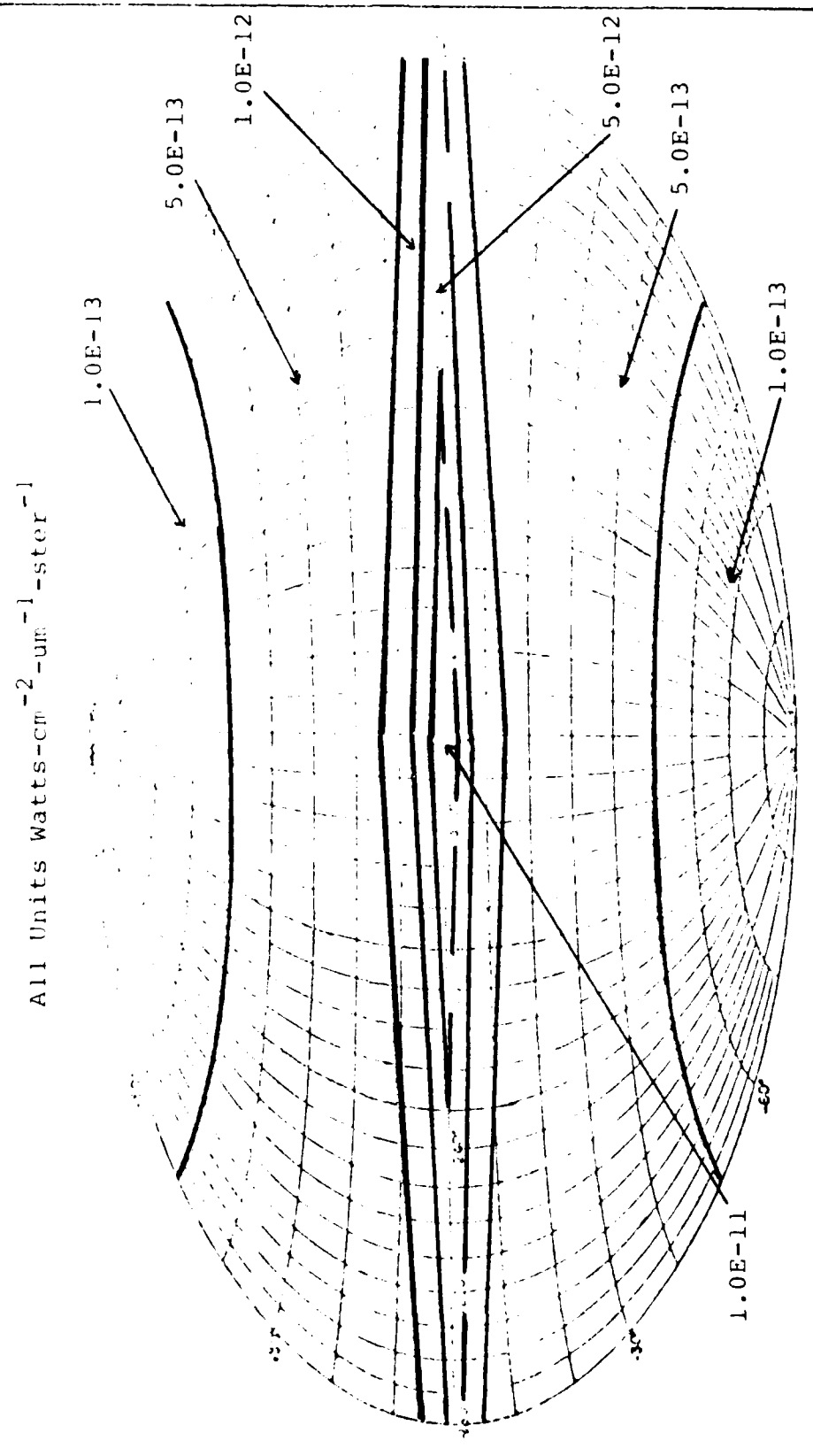
Figure 2. Radiance Contour Map

24

IV. SENSOR DESIGN

Various combinations of infrared detectors can be used to make up a sensor. Sensors can use a single detector, a linear array of detectors, or a two dimensional array of detectors as in a charge-coupled device (CCD). The matrix of detector cells can be spun around an axis to create a scanning sensor or may be stationary to create a staring array. The detector matrix can be held stationary and a reticle moved in front of the detectors to cause some angular or positional modulation of the incoming infrared radiation.

Detector cells for infrared light at around ten microns can be made of several combinations of materials. the most common being mercury-cadmium-telluride or silicon-arsenide. Silicon-arsenide was used on the IRAS sensor (20). Mercury-cadmium-telluride is used in the LANDSAT D thematic mapper and DMSP (12). Detector sensitivity varies with the material, but all must be cooled to cryogenic temperatures to be useful in a infrared sensor. This sensitivity, the quantum efficiency, is the average number of electrons produced per photon hitting the detector material. The quantum efficiency varies from about 10 to 50 per cent (19:1).

In order for an ASAT to successfully attack a target

spacecraft, the ASAT's sensor must acquire the target at a large enough distance so that orbital corrections can be made for intercept. The sensor's design must be sensitive enough to ensure reliable target detection, but not so complex that it becomes too expensive for a single use type mission.

Besides detector sensitivity, the spatial resolution of the sensor is also important. This is the ability to discriminate between two closely space objects. The resolution is a function of the size of the collecting optics the sensor, the detector size and spacing in the array, atmospheric seeing, and the wavelength of operation. For a sensor whose resolution is diffraction limited by its optics, the resolution θ

$$= 1.22 \frac{\lambda}{D} \tag{4.1}$$

where

λ = the operating wavelength and

D = the diameter of the optics.

is the angular distance in radians between the closest two objects that will be discernible as two objects instead of one object.

Resolution is not solely dependent upon optics, however; the number of detectors and their size determines the spatial resolution as well. If two point sources are

26

to be detected as two point sources, then their images must fall on two different detectors. The minimum resolvable angle θ

$$\theta = \frac{d}{F} \qquad (4.2)$$

where

d = the spacing between detectors,

F = the focal length of the optic system,

θ = the resolvable angle, in radians.

As an example, the infrared detector on LANDSAT D has a resolution of about 40 meters from a distance of 800 kilometers. If this same resolution existed for an ASAT sensor, the ASAT could distinguish between two targets a half a kilometer apart at a range of 10,000 kilometers. The ASAT should not need a resolution capability this fine however, because geosynchronous spacecraft are kept at least 600 kilometers apart (17).

Since the ASAT's sensor is expected to acquire the target at several hundred to several thousand kilometers distance, any target will be only a point source of infrared radiation. The assumed sensor will be operating with a wavelength bandpass around ten microns where most spacecraft with a temperature of 250 to 350 degrees K. radiate the most energy. The assumed target spacecraft

27

will radiate energy with intensity that is function of the emissivity of the surface and area facing the sensor.

In general, real spacecraft are not isotropic radiators. The amount of energy radiated is dependent upon the viewing angle and all the emissivities of the spacecraft outer components. Each different type of surface material - solar cells, antennas, insulation, paint, etc. - has its own emissivity. It is very difficult to predict the radiant characteristics of a particular target spacecraft whose projected area is constantly changing with respect to the viewing angle. Infrared irradiances for generic satellites at a temperature T are best described in terms of equivalent emissivity-areas.

In order to design a sensor for maximum efficiency, several factors must be considered:

S_R - the collecting area of the sensor,

$\eta(\lambda)$ - the quantum efficiency, that is, the number of measurable electrons generated per photon input to detector,

$\zeta_o(\lambda)$ - the percentage of radiation transmitted through the sensor optics,

λ_1, λ_2 - the spectral bandpass of the detector,

θ_R - the angle of incidence of the radiation onto the collecting area of the detector,

Ω_R - the field of view of the detector in steradians, and

28

T_s — the interval between samples of the detector output current.

The design of the sensor will determine all of these factors. One of the simplest sensors is a single detector with a spinning reticle. This is placed at the focal plane of the sensors optical system. The reticle consists of a circular mask with a single rectangular slit. A possible layout is shown in figures 3 and 4. The size of the reticle slit will determine how much of the detector is illuminated at any one time. When the reticle is spun about its center, objects appearing near the center of the reticle remain visible for a longer period of time than do objects near the edge of the reticle. It is this period of visibility coupled with the time that the object is seen in the rotation period that will determine the direction of the object relative to the axis of the sensor.

The output of the detector must be sampled often enough so the ASAT guidance system can make corrections in the trajectory if needed. The speed of the reticle rotation must be synchronized with the sampling rate so there are no gaps in coverage of the detector, yet positional accuracy is the best possible.

Since the size of the reticle slit determines how much of the total field of view the detector will see at any particular instant, it must be taken into account when

29
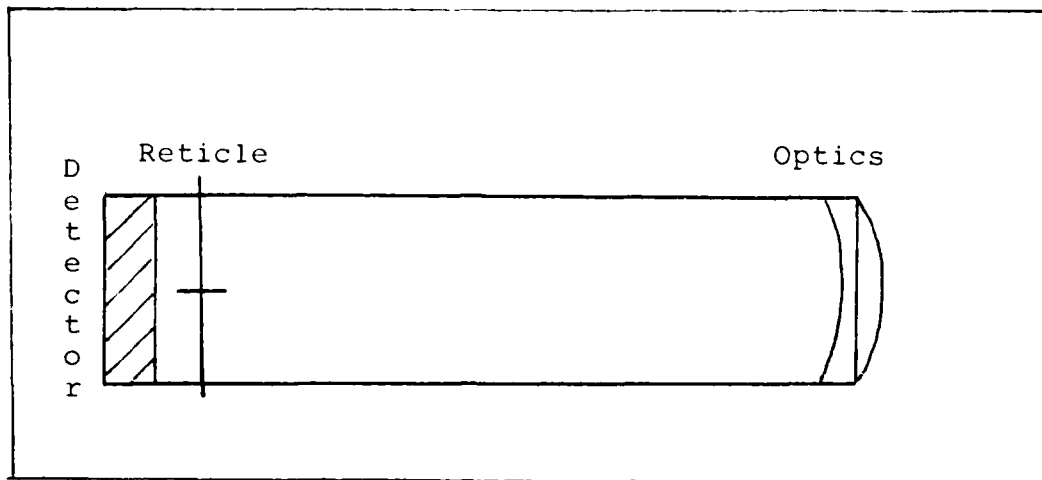
Figure 3.   Sensor Configuration
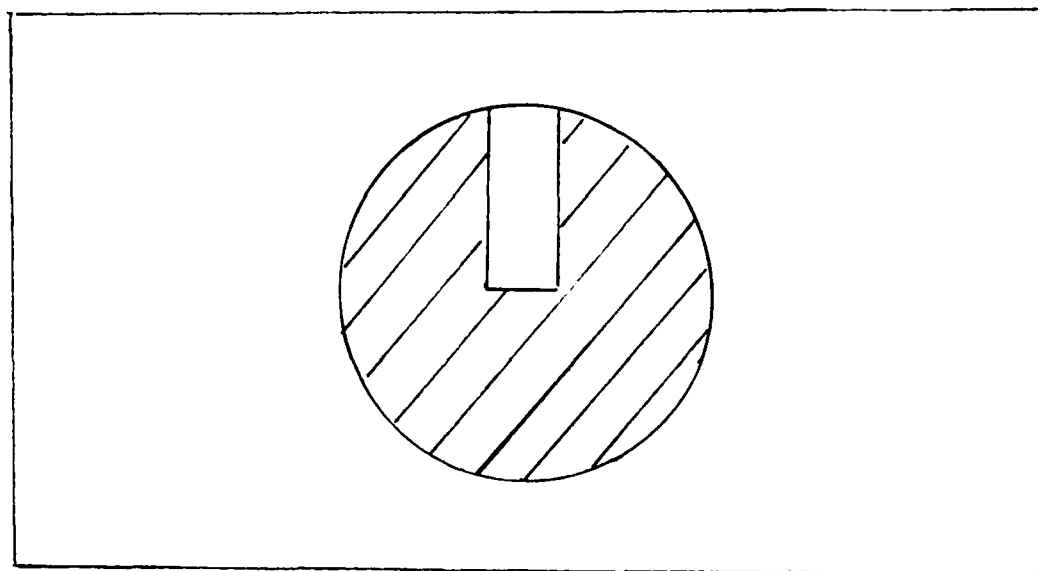
Figure 4.   Sensor Reticle

30

designing a possible ASAT sensor. That is, if the area of the reticle slit is 1/10th of the total area of the detector, the resulting instantaneous field of view of the sensor is only 1/10th of the total field of view of the optics.

The sampling time determines the positional accuracy of the sensor. The more often the output current is sampled, the finer resolution the sensor has. For example, a sensor with a reticle spinning ten rotations per second and reticle slit 20 degrees wide, the field of view is divided into 18 different sections. If the current is sampled four times during the time it takes the reticle to move twenty degrees, the current is sampled once every T_S = 1.39E-3 seconds. The sampling rate is the inverse of this, or about 720 times a second.

Since the output current is sampled every 5 degrees of reticle rotation, the positional accuracy relative to the circular scan, is 1/72 of the total scan. This breaks the field of view into 72 circular sectors. The positional accuracy relative to the distance along a radius of the detector face is more difficult to determine. Since the detector slit is rectangular, the part of the detector closest to the center is illuminated longer than portions near the outer edge. This means, if a target is close to the center of the optical axis, it will remain visible for more current samples than if the target was near the edge

31

of the field of view. For this sensor, targets at the edge of the field of view will be visible for 4 sampling periods while objects at the center will be visible for 32 sampling periods. This will divide the field of view into 28 different radial zones. The radial zones have more area toward the edge of the detector and less area toward the center. The circular sectors all have the same area.

It is the intersection of these sectors and zones that form the resolution element (see figure 5). The size of any resolution element is determined by its distance from the center of the detector. At a point half way out from the center, a target would be sampled 8 times per reticle revolution (see figure 5). The size of the radial zone having 8 samples per reticle field of view is about 17% of the total field of view. Since the field of view is also broken up into 72 circular sectors, multiplying 0.17 times 1/72 will give the part of the total field of view contained in this particular resolution element. This is about 0.0024. Since the total field of view is about 78.5 square degrees, this resolution element is about 0.434 degrees on a side.

The object of the ASAT sensor design is to determine how far away a proposed sensor can be from its target and still detect it reliably. The target must be detected against the infrared celestial background discussed in the previous section. To do this a series of calculations must

32
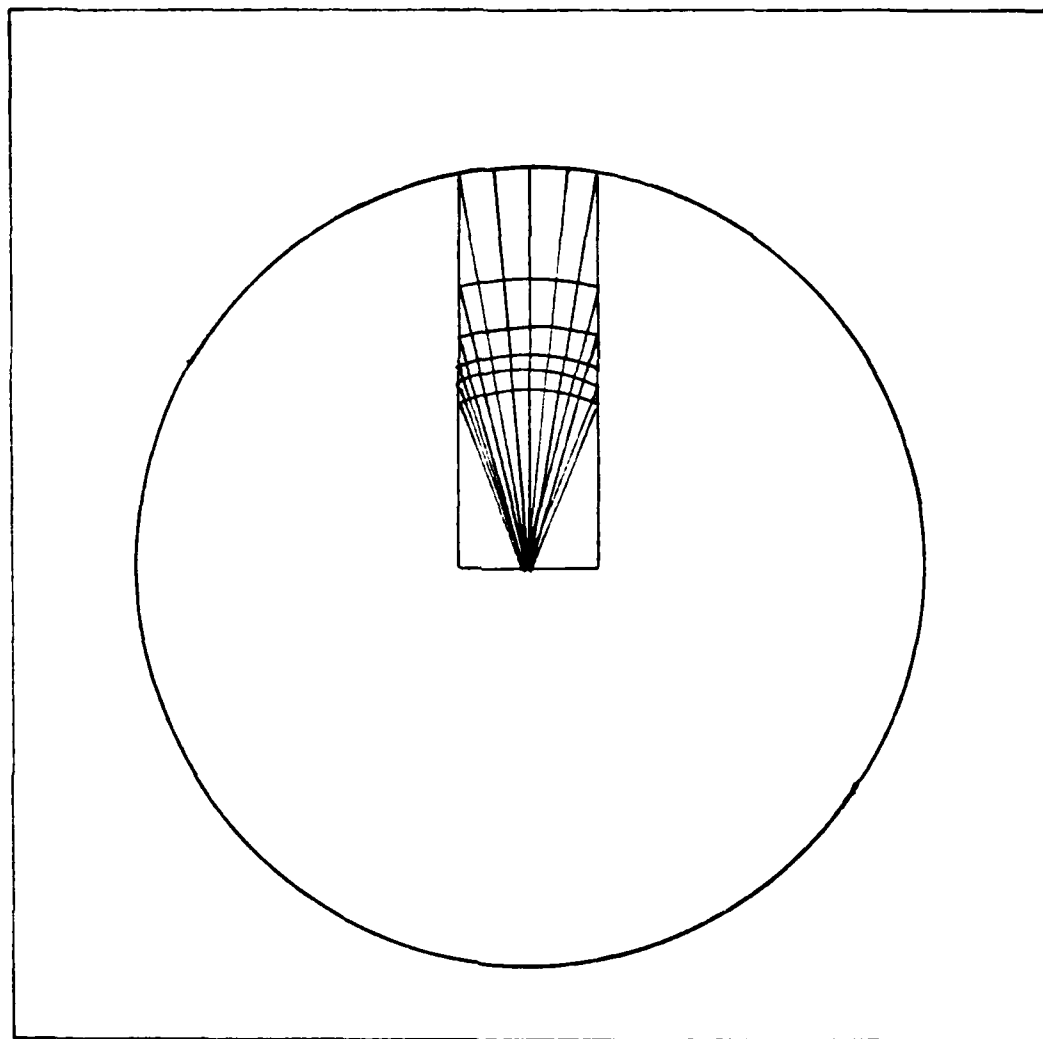
Figure 5. Resolution Elements

be performed. To perform these calculations, a set of
parameters for the proposed sensor must be used. They
involve the signal-to-noise ratio, the signal current
produced in the sensor from a target, and the signal
current produced in the sensor from the celestial
background. Table IV lists a set of possible sensor
parameters.

TABLE IV

Example ASAT Sensor Parameters

Optics Diameter = .2 meters, $S = \frac{\pi}{4} D^2 = 0.0314 \text{ m}^2$

Optics Cooled to 10° Kelvin

Optics Transmission - $\zeta_o = 0.9$

Field of View (Half Angle) = 5 degrees

Solid Angle $\Omega_{Fov} = \pi \theta^2 = 0.024$ Steradians

Detector: Si:As

NEFD = 1.0E-18 Watts-cm^{-2}

Focal Plane Cooled to 3° Kelvin

Cryogen: Liquid Helium

Detector Quantum Efficiency - $\eta(\lambda) = .25$

Detector Sample Rate = 720 samples per second

Reticle Spin Rate = 10 rotations per second

Reticle Slit Area = 11% of total detector

Wavelength Window = 9 to 13 microns

Average Wavelength $\bar{\lambda} = 11$ microns

Desired Signal-to-Noise Ratio - (S/N) = 5

From a point source target the amount of current i_T output from a detector (12),

$$i_T = \frac{e\,S_R\cos\theta_R}{hc\,r^2}\int_{\lambda_1}^{\lambda_2} I_\lambda(\lambda)\,\zeta_o(\lambda)\,\eta(\lambda)\,\lambda\,d\lambda \qquad (4.3)$$

where

I_λ = Target intensity in Watts/ster

e = charge on the electron, 1.6E-19 coulombs

h = Planck's constant, 6.62E-34 joule-sec

c = speed of light, 3.0E8 m/sec

r = range, the distance from the target to the sensor

From an extended background the amount of current i_B output from a detector is (12)

$$i_B = \frac{e\,S_R\,\Omega_R}{hc}\int_{\lambda_1}^{\lambda_2} L_\lambda(\lambda)\,\eta(\lambda)\,\zeta_o(\lambda)\,\lambda\,d\lambda \qquad (4.4)$$

where Ω_R is the solid angle of the filed of view and L is the background radiance in Watts-cm^{-2}-um^{-1}-ster .

To achieve reliable detection of a target the signal-to-noise ratio (S/N) must be high enough so the intermittent noise and background inhomogeneities do not frequently produce false targets. A signal-to-noise ratio

35

of five can guarantee few false alarms. The signal-to-noise ratio is defined as the average value of the current just from the target divided by the variance of the total current from the detector. The total current includes the target current, background current, and noise current. Specifically for a sensor using current for detection, where the only source of noise is photon noise, the signal-to-noise ratio is (37:541),

$$S/N = \frac{i_T}{\left(\left(i_T + i_B + i_D \right) 2 e \Delta f \right)^{\frac{1}{2}}}$$

(4.5)

where

i_T = total current

i_B = background current

i_D = dark or noise current

Δf = frequency bandwidth of the circuitry

e = charge of the electron

To design the sensor the analysis will proceed as follows:

1. Solve the Signal-to-Noise equation (eq. 4.5) for the Target Current i_T.

2. Solve the Target Current equation (eq. 4.3) for the Range.

3. Determine the Background Current from the Background

36

Current equation (eq. 4.4).

4. Determine the value of i_T obtained from the Signal-to-Noise equation (eq. 4.5).

5. Substitute the value of i_B to the Range equation (eq. 4.3).

6. Solve for the range r.

Since f is approximately equal to $\dfrac{1}{2\,t_S}$, where t_S the sampling time of the detector, the signal-to-noise ratio (12), becomes:

$$\frac{S}{N} = \frac{i_T}{\left((i_T + i_B + i_D)\,\dfrac{e}{t_s} \right)^{1/2}}$$

Solving for i_T yields:

$$i_T = \frac{\left(\frac{S}{N}\right)^2 \frac{e}{t_s} + \left(\left(\frac{S}{N}\right)^4 \left(\frac{e}{t_s}\right)^2 + 4\left(\frac{S}{N}\right)^2 \left(i_B + i_D\right)\frac{e}{t_s} \right)^{1/2}}{2}$$

The target current from an irradiance $I_\lambda(\lambda)$ is:

$$i_T = \frac{e\,S_R}{hc\,r^2} \int_{\lambda_1}^{\lambda_2} I_\lambda(\lambda)\,\zeta_0(\lambda)\,\zeta_A(\lambda)\,\eta(\lambda)\,\lambda\,d\lambda$$

Evaluating this across a small wavelength window near the peak of the blackbody curve gives:

$$i_T = \frac{e\, S_R\, \eta(\lambda)}{h\,c/\lambda \quad r^2}\, I_\lambda(\bar{\lambda})\, \zeta_o(\bar{\lambda})\, \zeta_A(\bar{\lambda})\, \Delta\lambda$$

This assumes $\eta(\lambda),\, \zeta_o(\lambda),\, \zeta_A(\lambda)$ are constant across the window. Since the sensor is outside of the atmosphere $\zeta_A(\bar{\lambda}) = 1.0$. On IRAS $\zeta_o(\bar{\lambda})$ was about 0.9, which is the value assumed here (20). This leads to:

$$i_T = \frac{e\, S_R\, \eta(\bar{\lambda})}{h c/\lambda \quad r^2}\, \zeta_o(\bar{\lambda})\, I_\lambda(\bar{\lambda})\, \Delta\lambda$$

The irradiance from a point source is:

$$\mathcal{E}_T = \frac{1}{r^2} \int_{\lambda_1}^{\lambda_2} I_\lambda(\lambda)\, d\lambda = \frac{1}{r^2}\, I_\lambda(\bar{\lambda})\, \Delta\lambda$$

Substituting for $I_\lambda(\bar{\lambda})$,

$$i_T = \frac{e\, S_R}{h c/\lambda}\, \eta(\bar{\lambda})\, \zeta_o(\bar{\lambda})\, \mathcal{E}_T$$

The maximum energy output is determined by the Planck function (12)

$$B_\lambda(\lambda, T) = \frac{2\pi h c^2}{\lambda^5} \quad \frac{1}{\exp\left(hc/\lambda k T - 1\right)}$$

38

where

  T = the objects temperature in degrees Kelvin,

  h = Planck's constant,

  c = the speed of light,

  λ = the wavelength, and

  k = Boltzmann's constant = 1.38E-23

    Joules/molecule-degrees K.

Given a standard target, one with a temperature of 300 degrees Kelvin and an emissivity-area equal to 1 square meter, and a spectral irradiance at a distance r the Planck function yields a spectral radiance L for wavelengths $9 \leq \lambda \leq 13$ microns,

$$L_\lambda = \frac{30}{\pi} \text{ Watts-m}^{-2}\text{-ster}^{-1}\text{-um}^{-1}$$

$$\varepsilon_\lambda = \frac{30}{\pi r^2} \text{ Watts-m}^{-2}\text{-um}^{-1}$$

For a four micron bandwidth from 9 to 13 microns, the irradiance E integrated over the spectral bandpass,

$$\varepsilon_T = \frac{120}{\pi r^2} \text{ W-m}^{-2}$$

Therefore,

$$\lambda_T = \frac{120 \, e \, S_R \, \eta(\lambda) \, \tau_o(\lambda)}{^{hc}\!/\!_\lambda \, \pi r^2}$$

39

Solving this equation for the range r,

$$r = \left(\frac{120 \, S_R \, \eta(\bar{\lambda}) \, \zeta_o(\bar{\lambda})}{hc/\bar{\lambda} \; \pi \; i_T/e} \right)^{1/2}$$

The background contribution to the signal-to-noise equation must be determined. The background current when evaluated,

$$i_B = \frac{e \, S_R \, \Omega_R}{hc/\bar{\lambda}} \, \eta(\bar{\lambda}) \, \zeta_o(\bar{\lambda}) \, L_\lambda(\lambda) \, \Delta\lambda$$

where $\Delta\lambda = \lambda_2 - \lambda_1$ = the sensor wavelength bandpass. This assumes $\eta(\lambda)$ is constant across the bandwidth and is the average wavelength (11 microns). From calculations in the previous section, the amount of background radiance L_{B_λ} at eleven microns varies from about 1.0E-11 to 1.0E-13 W-cm^{-2}-um^{-1}-ster^{-1}.

The solid angle Ω_{FOV} is that portion of the field of view observed by the sensor at any instant in time. Since the reticle slit only allows about 11% of the total field of view to reach the detector, $\Omega_R = 0.11 \, \Omega_{FOV}$.

For various values of L_B the above equation gives the values for i_B in table V.

TABLE V

Sensor Current

BACKGROUND SPECTRAL RADIANCE = L_{β_λ}	CURRENT i_β
1.0E-11 Watts-cm^{-2}-um^{-1}-$ster^{-1}$	7.37E-11 amps
1.0E-12	7.37E-12
1.0E-13	7.37E-13

The dark current contribution to the signal-to-noise equation must be determined. The dark current is the combination of two factors. First there is the detector output current when no photons are incident. Second, there is the detector output current from infrared radiation given off by the rest of the sensor, i.e. optics, tube, baffles, etc. By cooling both the detector and the sensor components, this noise can be kept to a minimum, but not entirely eliminated. For the IRAS sensor the system in-band noise equivalent flux density was 1.0E-19 watts-cm^{-2} (20:69). This value included the system noise from the detectors, amplifiers, and filters. The proposed sensor is about 1/10 a large as IRAS, therefore, the proposed sensor's NEFD will be about 10 times that of IRAS, 1.0E-18 watts-cm^{-2}. Since this value is much less than background irradiances, the dark current can be neglected for the accuracy desired in this investigation.

Now that the values needed for the range calculation are available, the maximum range an ASAT can be from its target and still detect the target can be found.

Assuming a signal-to-noise ratio of five, a sample time T_S of 1.39E-3 seconds, and minimum background current of 7.37E-13 amps, the equation

$$i_T = \frac{(S/N)^2 \frac{e}{t_s} + \left((S/N)^4 \left(\frac{e}{t_s}\right)^2 + 4(S/N)^2 (i_B)\left(\frac{e}{t_s}\right) \right)^{1/2}}{2}$$

gives a value of i_T = 4.74E-14 amps.

Solving for the range equation below using the values from Table IV,

$$r = \left(\frac{120 \, S_R \, \eta(\lambda) \, \zeta_o(\lambda)}{hc/\lambda \, \pi \, i_{T}/e} \right)^{1/2}$$

Gives the maximum range of 7271 kilometers. Table VI lists ranges for other values of background radiances.

TABLE VI

Maximum Ranges versus Background Radiances

Background - Watts-cm^{-2}-um^{-1}-$ster^{-1}$	Range-Kilometers
Spectral Radiance L_{β_λ}	R
1E-13	7271
2E-13	6143
3E-13	5563
4E-13	5184
5E-13	4907
6E-13	4691
7E-13	4516
8E-13	4369
9E-13	4244
1E-12	4135
2E-12	3482
3E-12	3149
4E-12	2931
5E-12	2773
6E-12	2650
7E-12	2250
8E-12	2467
9E-12	2396
1E-11	2333

V. MODEL ACCURACY

The values of the maximum sensor detection ranges derived the the previous chapter depend upon the accuracy of the Walker Sky Model. While this model is based upon actual observational data, the model's accuracy may be questioned from several different angles. Specifically three questions are raised:

1) Does the model include all the stars that have a significant contribution to the sky radiance?

2) How does the number of infrared sources predicted by the model compare with cataloged observations?

3) What non-stellar infrared sources must be added to obtain true sky radiance values?

This chapter will answer the first two questions. The next chapter will answer the last question.

Limiting Irradiance Effects

The sky model data only lists stars down to an irradiance level of $1.0E-20$ Watts-cm^{-2}-um^{-1}. To determine if fainter stars contribute to the sky radiance, the data in Table II can be examined. For each galactic position, the number of sources increases with decreasing spectral irradiance. The number of sources for each entry is the total number of sources at that particular irradiance level and brighter. It is the number of sources times the irradiance level that determine the individual irradiance

level contributions to the total sky radiance.

In examining the columns of data, the number of sources increase by an order of magnitude or more for each decreasing irradiance level only at low galactic latitudes. At higher latitudes, the number of sources increases rapidly at first and then levels off as irradiance level of $1.0E-18$ watts-cm^{-2}-um^{-1} is reached. Evaluating this trend leads to the conclusion that the number of sources appears to be rather finite at high galactic latitudes and that fainter irradiance levels than $1.0E-20$ will not contribute to the model for that sky region. Figure 6 shows this trend by plotting number versus irradiance. Figure 7 shows this by plotting the contribution to the total radiance by each irradiance range.

At galactic latitudes of zero and two degrees, the number of sources does not level off. This indicates that at fainter irradiance levels than $1.0E-20$ watts-cm^{-2}-um^{-1}, additional sources may be of sufficient number to contribute significantly to the model. For example, at an irradiance level of $1.0E-21$ an estimate of the number of sources of $1.0E6$ is possible if the trend from irradiance levels $1.0E-19$ and $1.0E-20$ is followed. This is shown graphically in figures 8 and 9.

How faint this analysis should be taken is limited to those irradiance levels that make significant contributions to the model. The contribution for irradiance level 1.0E-
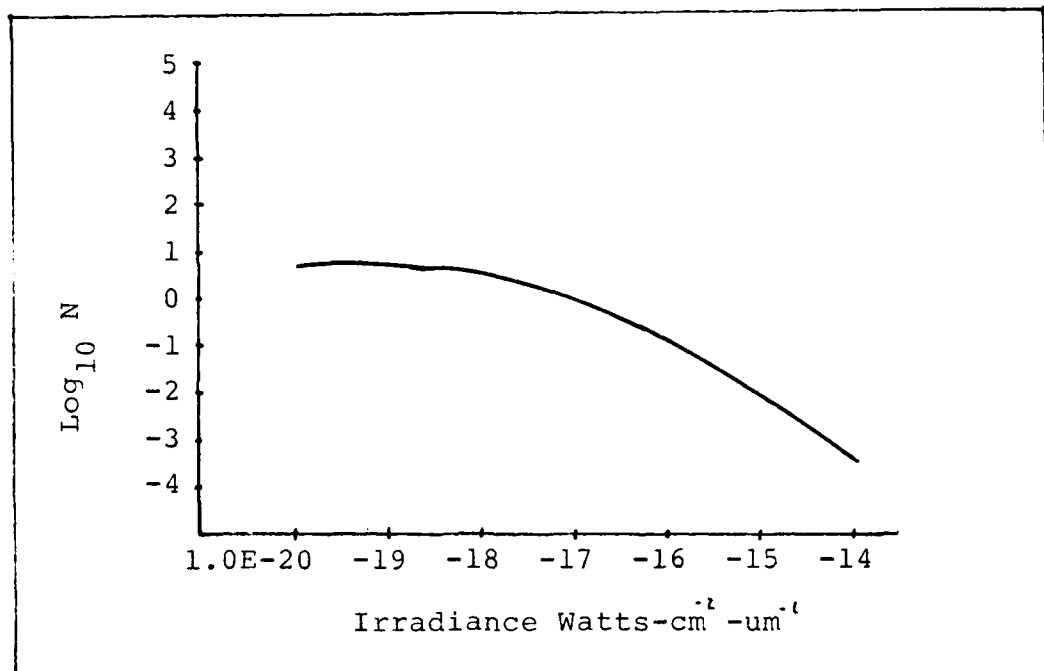
Figure 6.   Number of Sources vs Irradiance Range

Galactic Latitude 20 Longitude 90
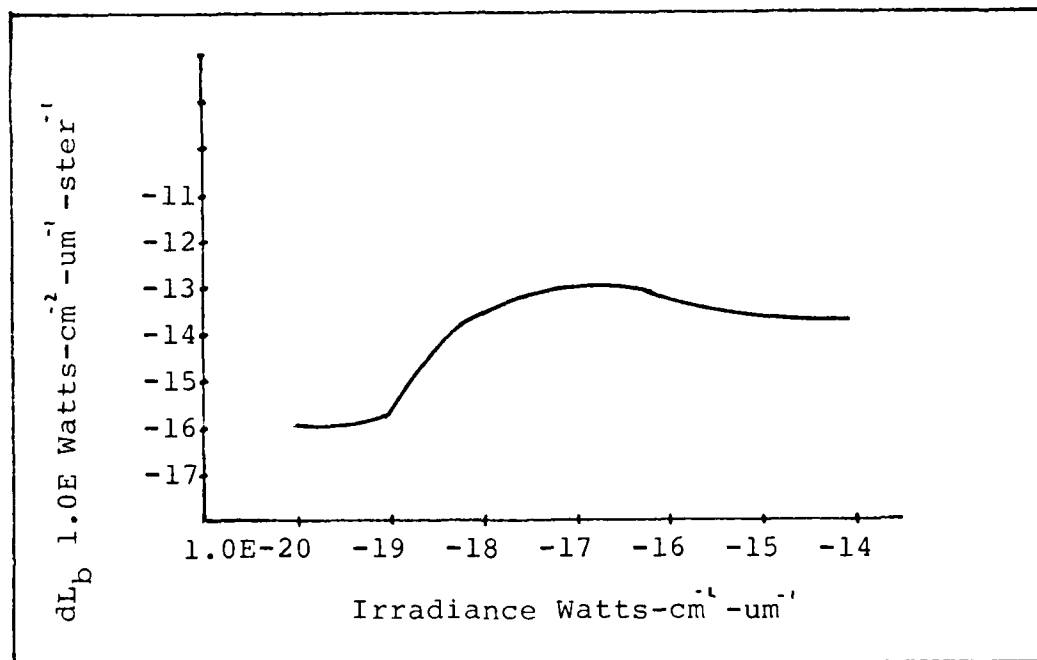
Figure 7.   Change in Radiance vs Irradiance Range

Galactic Latitude 20 Longitude 90

46
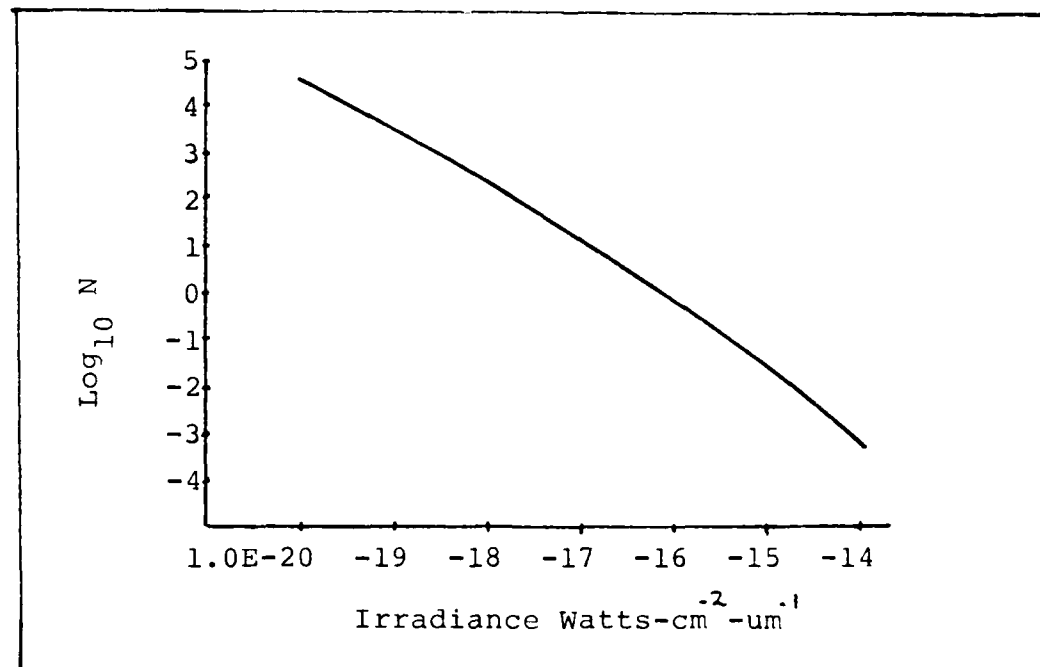
Figure 8.   Number of Sources vs Irradiance Range

Galactic Latitude 0 Longitude 90
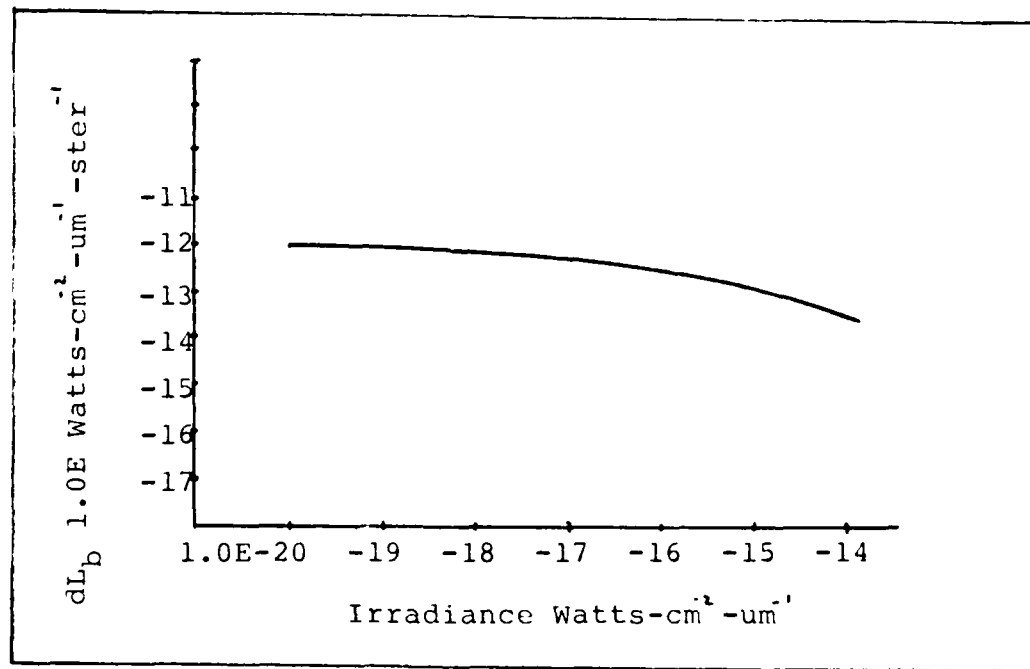
Figure 9.   Change in Radiance vs Irradiance Range

Galactic Latitude 0 Longitude 90

47

21, for latitude 0, longitude 0, is estimated to be as follows:

$$(1.0E6 - 1.0E5) \times 1.0E-21 = 9.0E-16 \ W\text{-}cm^{-2}\text{-}um^{-1}$$

The radiance value for this area was previous calculated to be 5.0E-15. This means that the estimated contribution from irradiance level 1.0E-21 is about a 20 percent increase over the previously calculated value.

This process can be extended to irradiance level 1.0E-22, but this level will require the number of sources to be on the order of 1.0E7 if it is to make the same contribution to the radiance. Since the Milky Way galaxy has an estimated hundred billion stars in it (1), expecting ten million stars to be visible while looking through the galactic center is not unreasonable. However, the actual number of stars detectable will be limited by interstellar dust and gas clouds. So it is very difficult to predict when there are no more fainter stars that will contribute to the model.

In summary, the model seems accurate at latitudes greater than two degrees. On the galactic plane the radiance values previous calculated in Table IV could be in error. Determination of the magnitude of the error will be left to an examination of actual observations.

Comparison to Observations

The comparison to actual infrared observations at around 10 microns is divided into two parts: 1) a

48

comparison with data from the AFGL catalog data, and 2) a comparison with IRAS preliminary results.

The AFGL catalog of infrared stars has some gaps in its coverage. These gaps are not large at 10 microns, but must be considered when choosing areas of the sky for the comparison. Four areas of the sky were chosen. These areas are 15 degrees on a side and represent two areas along the galactic plane, and two areas at high galactic latitude. The approximate centers of the areas are listed in Table VII. The areas are plotted in galactic coordinates in figure 10.

TABLE VII

Centers of Selected Sky Areas

Area	Galactic Latitude	Galactic Longitude	Right Ascension	Declination
1	0	30	1900	0
2	5	210	0700	0
3	60	270	1200	0
4	-60	90	0000	0

Appendix B contains the list of stars for each area with their AFGL catalog number, right ascension, declination, and magnitude. Also in Appendix B is a graphic plot of the stars in each area. A magnitude of 0.0 equates to 8.3E-17 Watts-cm^{-1}-um^{-1} at 11 microns. A discussion of magnitudes and irradiance used in this thesis
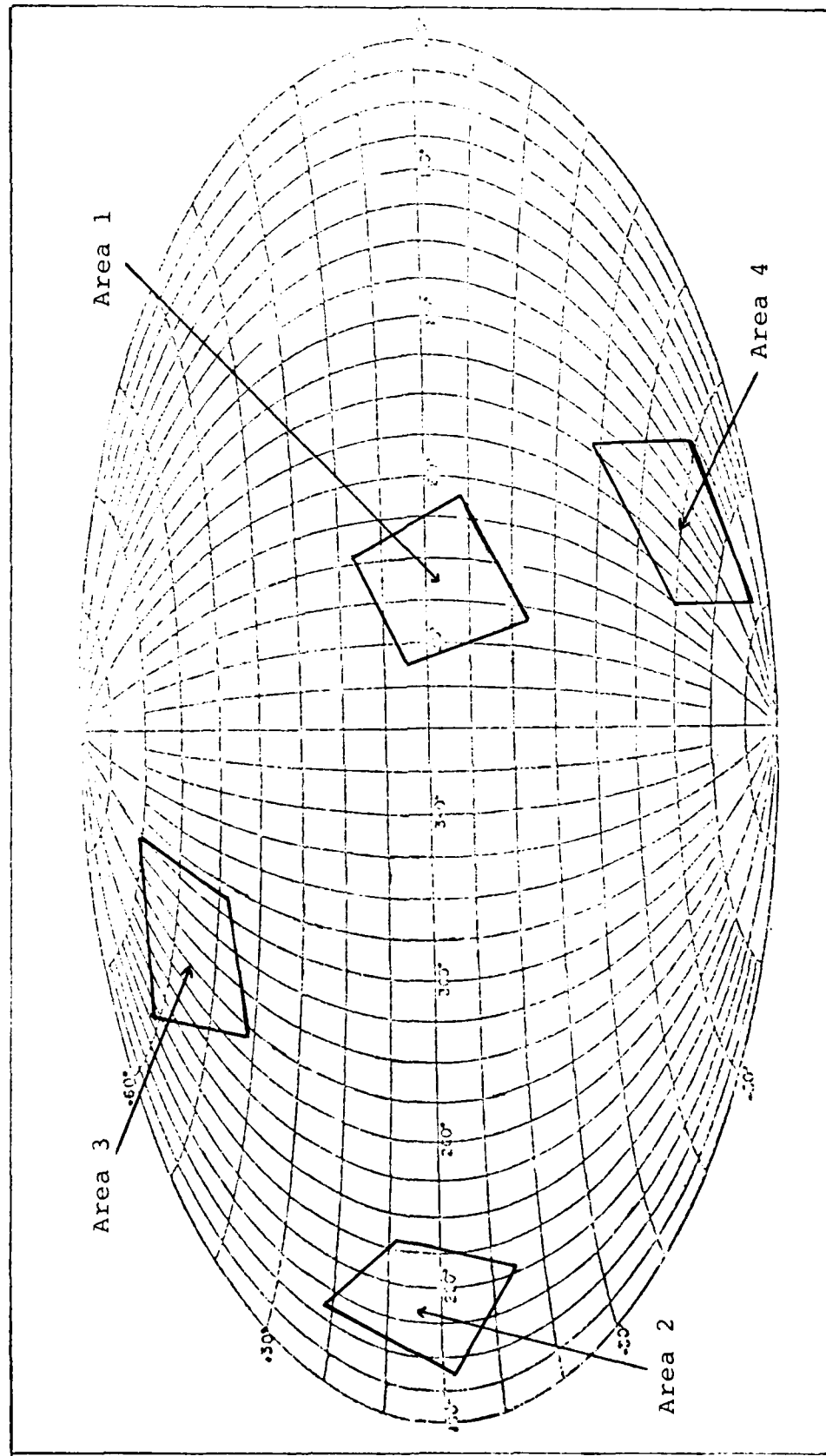
Figure 10. Selected Sky Areas in Galactic Coordinates

is in Appendix C.

Table VIII shows the radiance value calculated for each area based upon the number of stars and their respective irradiances. Also in this table is the radiance value predicted by the Walker Sky Model. There is general agreement between prediction and AFGL catalog data away from the galactic plane, but on the plane the model predicts more radiance than the catalog data indicates. This is because the AFGL catalog only contains sources at faint as $1.0E-16$ Watts-cm^{-2}-um^{-1} and lacks the vast number of faint sources in the plane of the galaxy.

It is also possible to relate the number of sources predicted with AFGL catalog data at those irradiance levels for which the catalog has data. The AFGL catalog has data for irradiance levels of $1.0E-14$, $1.0E-15$, and $1.0E-15$ Watts-cm^{-2}-um^{-1}. For the four areas previously mentioned, Table IX shows the comparison between the number of source predicted from the Walker Sky Model versus the actual number of sources per square degree from the AFGL catalog. The values of actual and predicted usually agree with a factor of ten. The best agreement occurs at an irradiance level of $1.0E-16$ Watts-cm^{-2}-um^{-1}.

To summarize, the Walker Sky Model does agree roughly with 11 micron data present in the AFGL catalog. This is not surprising since the model is based partly on the data in this very catalog. However, the number of sources

predicted is an average based upon data for the entire sky, and cannot be expected to agree precisely for any one region.

TABLE VIII

Radiance Comparison Measured in Watts-cm^{-2}-um^{-1}-ster^{-1}

Area	Radiance Predicted by Walker Sky Model	Radiance from AFGL Catalog Data
1	2.1E-11	2.3E-12
2	1.7E-12	3.3E-13
3	9.4E-14	1.2E-13
4	9.4E-14	7.7E-14

TABLE IX

Sources per Square Degree

Comparison of Predicted versus AFGL Catalog

Irradiance Levels are Watts-cm^{-2}-um^{-1}

	Irradiance Level	Predicted	AFGL Catalog
Area 1	1.0E-14	5.6E-4	8.9E-3
	1.0E-15	1.9E-2	6.2E-2
	1.0E-16	7.1E-1	5.0E-1
Area 2	1.0E-14	5.4E-4	0.0
	1.0E-15	1.4E-2	8.8E-3
	1.0E-16	1.4E-1	1.4E-1
Area 3	1.0E-14	1.3E-4	0.0
	1.0E-15	2.8E-3	0.0
	1.0E-16	7.0E-2	6.2E-2
Area 4	1.0E-14	1.3E-4	0.0
	1.0E-15	2.8E-3	0.0
	1.0E-16	7.0E-2	4.4E-2

The comparison of the Sky Model results with IRAS data is more difficult because preliminary data from IRAS is all that is currently available. This data consists of a small catalog of stars detected by the IRAS "minisurvey" conducted before the general observation program began (22), and some initial analysis of this data (29).

The IRAS minisurvey consisted of a survey of 300 square degrees between galactic latitude 20 to 40 degrees. The data set is considered 95% complete down to an irradiance level 0f $2.1E-18$ Watts-cm^{-2}-um^{-1} (22:C1). For the minisurvey region at 12 microns, the density of sources brighter than $2.1E-18$ Watts-cm^{-2}-um^{-1} is estimated to be 1.1 per square degree (29:L7). This agrees within a factor of two with the value predicted by the Sky Model (see table II) for an irradiance level of $1.0E-18$ Watts-cm^{-2}-1-um^{-1} for a galactic latitude of 30 degrees at 11 microns. Analysis of the number of sources versus irradiance shows there are more sources at lower values of irradiance than higher values of irradiance, which agrees with the sky model (29:L8).

An additional point of reference is two scans conducted by IRAS that crossed the galactic plane (29:L7). The two scans were at galactic longitudes 144 and 338 degrees respectively. The number of sources detected by averaging these two scans is shown in figure 11. The limiting irradiance for this figure is $2.1E-18$ Watts-cm^{-2}-

53
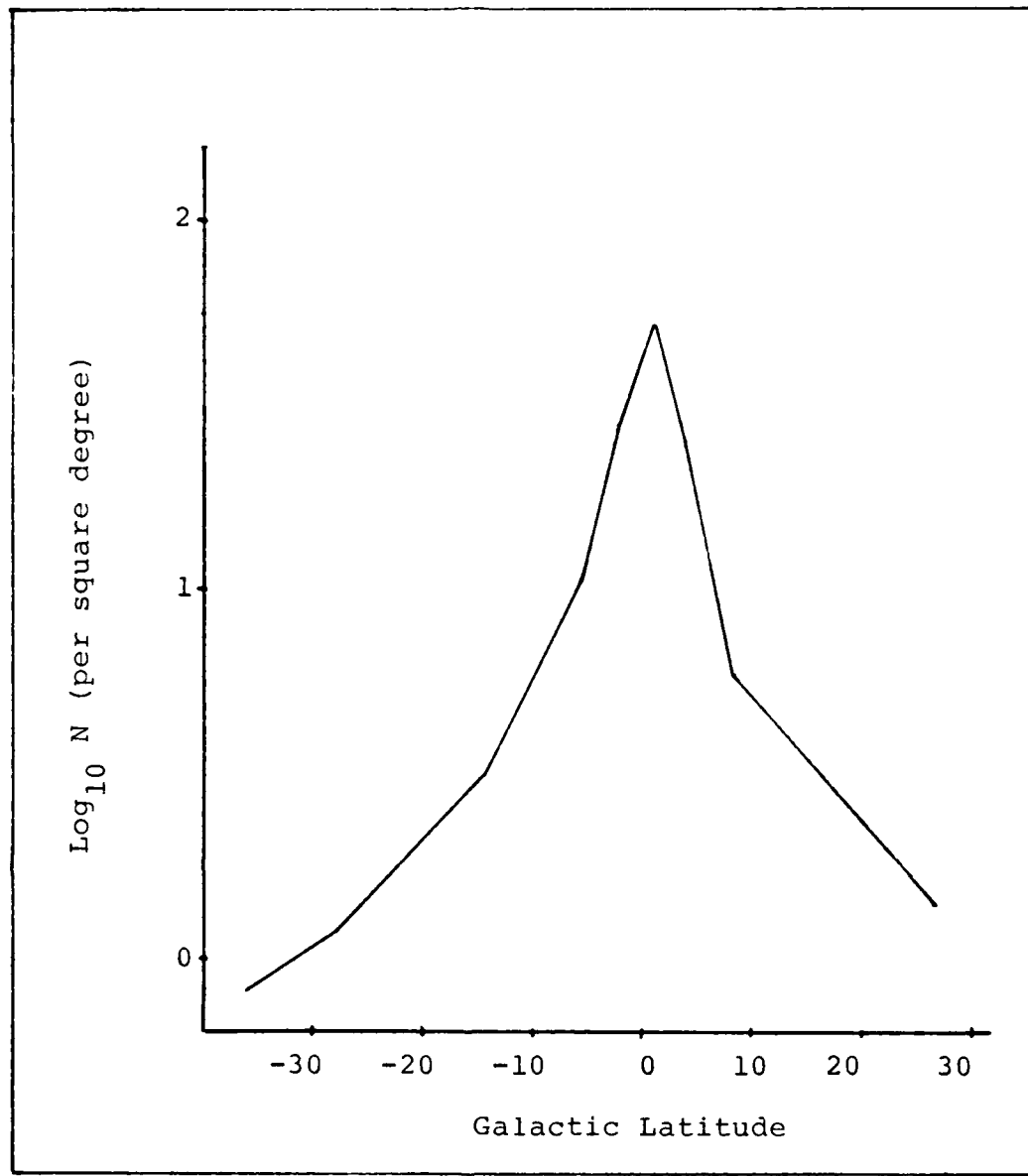
Figure 11.   Number of Sources per Square
             Degree.   IRAS Data at Longitudes
             144 and 338. Note general
             agreement between this data and
             Walker Sky Model.

um^{-1}. The number of sources detected is similar to those predicted by the Sky Model for this irradiance level and a longitude of 144 degrees, and latitudes greater than five degrees. However, the number of sources detected in the center of the galactic plane is about 50% less than that predicted by the model.

The stars detected by the IRAS minisurvey source catalog are listed in Appendix B. The total radiance from these stars for the area of the survey is 1.1E-13 Watts-cm^{-2}-um^{-1}-ster^{-1}. This is a factor of five less than the sky model prediction for galactic latitudes between 20 and 40 degrees. This may be due to the fact that the data catalog only contains stars which were detected by IRAS with an irradiance of at least 2.1E-18 Watts-cm^{-2}-um^{-1} and fainter stars can contribute to the total radiance for that region. The Walker Sky Model minimum irradiance level is 1.0E-20 Watts-cm^{-2}-um^{-1}.

A reliable estimate of the radiance of the galactic plane from the sky model or from discrete source catalogs is difficult to determine. The analysis of whether the sky model includes stars faint enough shows that stars fainter than 1.0E-20 Watts-cm^{-2}-um^{-1} could make significant contributions to the total radiance along the galactic plane. However, discrete source observations fail to confirm the model prediction of radiance in the galactic plane. Price (25) has developed some low resolution maps

55

of the galactic plane where total flux received by the
sensor is plotted and not just discrete sources. The data
is from the AFGL sounding rocket flights. These maps
indicate the galactic plane varies in radiance from 4.7E-11
Watts-cm^{-2}-um^{-1}-ster^{-1} at 0 degrees galactic latitude to
7E-12 Watts-cm^{-2}-um^{-1}-ster^{-1} at 5 degrees latitude. These
values are about the same as those predicted by the sky
model.

VI.   Additions to the Model

As stated in the introduction to this thesis, sources
of celestial infrared radiation include not only stars, but
planets, asteroids, interplanetary dust, and interstellar
gas. Each contributes to the infrared background. It goes
without saying that the Sun is the most intense source of
infrared radiation, but any sensor looking directly into
the sun would be instantly, and probably permanently,
blinded.

All the planets of our solar system (including the
earth) emit infrared radiation in the range around ten
microns. The inner planets are the strongest sources, with
irradiances falling as distance from the sun increases.
The point source irradiances near the earth from a few
planets at their mean earth-planet distances are: Venus:
$6.22E-12$ W-cm^{-2}, Mars: $3.53E-13$ W-cm^{-2}, Jupiter: $7.40E-14$
W-cm^{-2} and, Saturn: $2.24E-17$ W-cm^{-2}.

The planets themselves should not cause many problems
for an ASAT sensor. The positions of the planets (the
earth and moon as well) can be determined ahead of time
and the ASAT interception orbit adjusted so the ASAT sensor
never sees a planet. If this isn't possible, the ASAT
sensor must be "smart" enough to know when it should see a
planet and then ignore it as a target.

Asteroids are solid objects orbiting the Sun. Most of

57

them lie in orbits between the orbits of Mars and Jupiter. Asteroid surface temperatures vary from about 180 to 280 degrees Kelvin with a mean of about 256 degrees (36:3-31). While this is a little cooler than normal satellite temperatures, asteroids still radiate a substantial amount of energy at around ten microns.

Asteroids, like planets, are confined to a portion of the sky along the ecliptic. The ecliptic is a line around the sky inclined 23 and 1/2 degrees with respect to the celestial equator. A graph of the ecliptic plane in galactic coordinates is shown in figure 12. Ecliptic coordinates are discussed in Appendix A. The asteroids are confined to a band about thirty degrees wide, centered on the ecliptic. Within this band asteroids will raise the value of the infrared sky radiance.

Walker (36:3-33) has developed a model, based upon the data from Murdock (21), to estimate the number of asteroids present per square degree of sky. The model was developed from asteroids observed in the infrared, and orbital data on 1800 known asteroids. This model for eleven micron radiation is:

$$N = 4.6E-19 \ E_\lambda \ \exp(-0.14 \ B_e)$$

where

N = the number of asteroids per square degree to a limiting irradiance E_λ,

E_λ = the limiting irradiance in Watts-cm^{-2}-um^{-1}, and

58
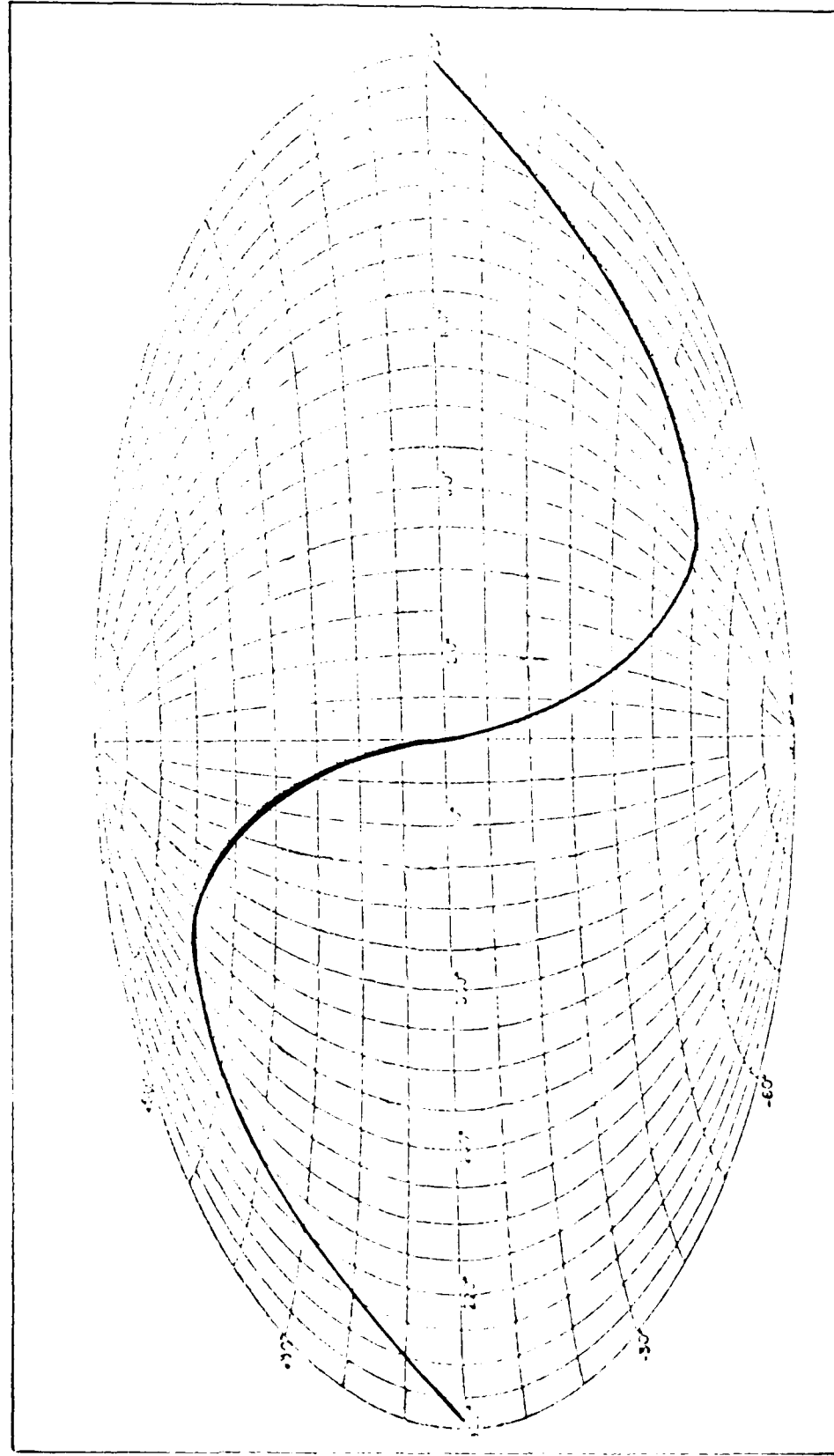
Figure 12. Ecliptic in Galactic Coordinates

59

B_e = the ecliptic latitude in degrees.

Evaluating this model for various ecliptic latitudes yields the data shown in Table X. Radiance values calculated from this model in Watts-cm^{-2}-um^{-1}-ster^{-1} is shown in Table XI.

TABLE X

Number of Asteroids per Square Degree

Irradiance	Ecliptic Latitude				
	0	5	10	15	20
1E-14	4.6E-5	2.3E-5	1.1E-5	5.6E-6	2.8E-6
1E-15	4.6E-4	2.3E-4	1.1E-4	5.6E-5	2.8E-5
1E-16	4.6E-3	2.3E-3	1.1E-3	5.6E-4	2.8E-4
1E-17	4.6E-2	2.3E-2	1.1E-2	5.6E-3	2.8E-3
1E-18	4.6E-1	2.3E-1	1.1E-1	5.6E-2	2.8E-2
1E-19	4.6E0	2.3E0	1.1E0	5.6E-1	2.8E-1
1E-20	4.6E1	2.3E1	1.1E1	5.6E0	2.8E0
1E-21	4.6E2	2.3E2	1.1E2	5.6E1	2.8E1

Irradiance is in Watts-cm^{-2}-um^{-1}

TABLE XI

Radiance from Asteroids in Watts-cm^{-2}-um^{-1}-$ster^{-1}$

Ecliptic Latitude	Radiance
0	2.2E-14
5	1.1E-14
10	5.5E-15
15	2.7E-15
20	1.3E-15

The radiance for asteroids is brightest along the ecliptic plane. The contribution is at best only about 25% of the stellar component predicted by the Walker model at galactic latitude of 60 degrees and higher. While the asteroid contribution to the background may seem possibly important for sky regions away from galactic plane, its contribution is small compared to the contribution from zodiacal light particles.

The infrared radiation from zodiacal light particles is thought to come from particles that range in size from 10 to 100 microns. These particles are evenly distributed in the vicinity of the earth's orbit (14:183). The particles are at a temperature of about 250 degrees Kelvin (11:L17). The amount of infrared radiation emitted from the zodiacal light particles varies as a function of angular distance from the ecliptic plane, and as a function of angular distance from the Sun (elongation angle).

The analysis of the radiance from zodiacal light particles is not complete. The best data available is from Price, Murdock, and Marcotte (24:765), and from Hauser, et al (11:L15). The observations by Price are based upon sounding rocket flights for the AFGL Sky Survey. The Hauser data is based upon scans made by IRAS.

Both the Price and Hauser data analyses indicate that the radiance in the ecliptic plane is much larger than the radiance from the stellar background. At an elongation angle of 75 degrees, Price puts the infrared radiance at 11 microns at about 7.0E-11 Watts-cm^{-2}-um^{-1}-ster^{-1}. Hauser indicates at 12 microns the value is about 1.0E-10 Watts-cm^{-2}-um^{-1}-ster^{-1} at the same elongation angle. The main difference between the two data sets is the value of the radiance away from the ecliptic plane. The IRAS data indicates that the radiance at the ecliptic poles is about at least five times as large as the sounding rocket data for the ecliptic poles. Which data is correct is still open to debate. A sample of data from both sources is listed in tables XII and XIII. The tables are not at the same elongation angle. A plot of radiances versus elongation angle is shown in figure 13. The data for figure 13 is from Price (24) and Hauser (11).

TABLE XII

Zodiacal Emission

Infrared Radiance Based Upon Sounding Rocket Data(24)

Elongation Angle of 75 Degrees

Ecliptic Latitude	Intensity at 11 Microns Watts-cm^{-2}-um^{-1}-ster^{-1}
-30	1.1E-11
-20	1.7E-11
-10	4.3E-11
- 5	5.7E-11
0	6.8E-11
5	5.9E-11
10	4.3E-11
20	1.8E-11
30	1.3E-11

TABLE XIII

Zodiacal Emission

Infrared Radiance Based Upon IRAS Observations(11)

Elongation Angle of 90 degrees

Ecliptic Latitude	Radiance at 12 Microns Watts-cm^{-2}-um^{-1}-ster^{-1}
-71	4.6E-11
0	1.6E-10
80	3.7E-11
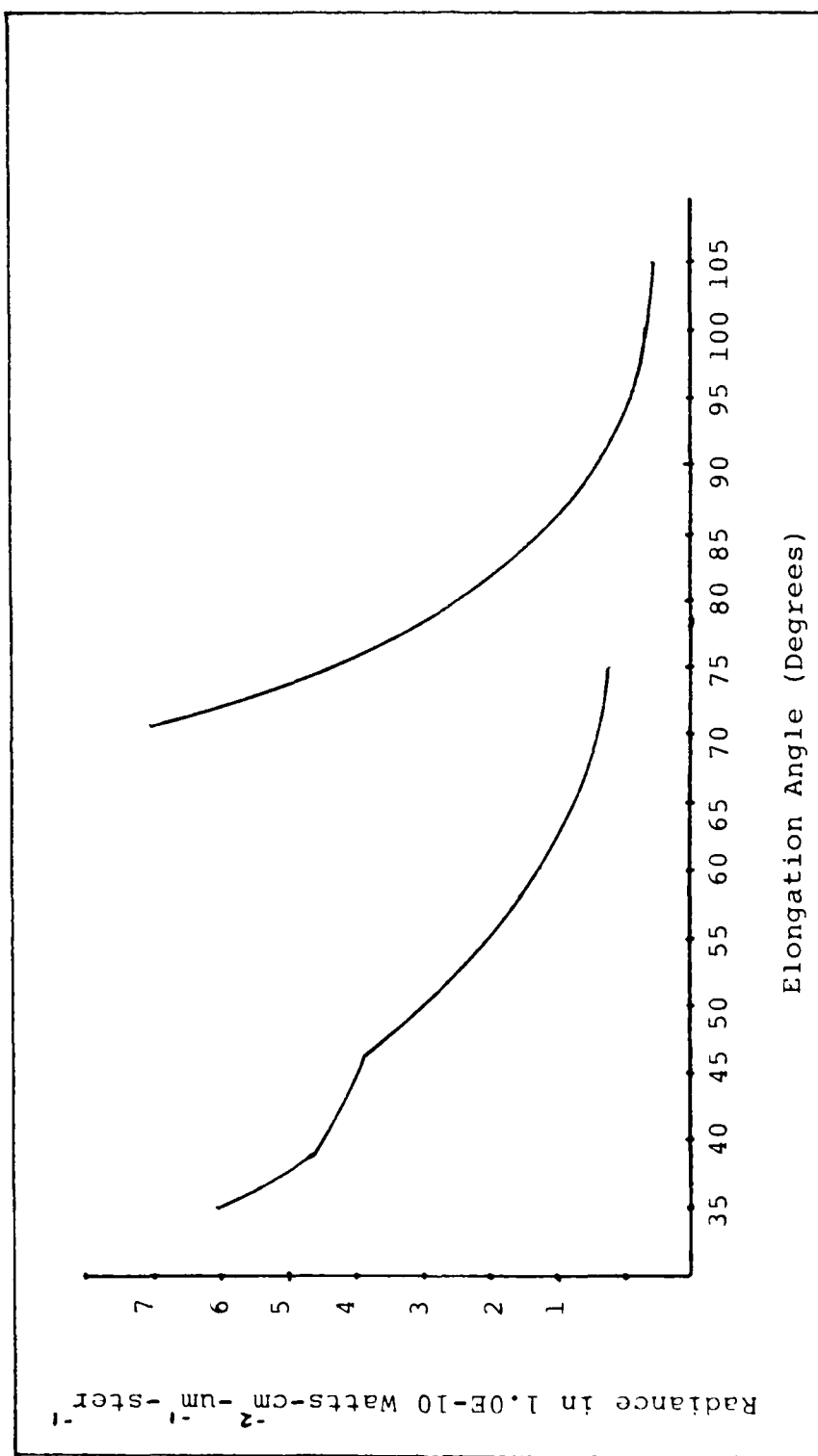
Figure 13. Zodiacal Radiance vs Elongation Angle

Radiance from Sounding Rocket Data (left) (24)
Radiance from IRAS Data (right) (11)
Ecliptic Latitude 0 Degrees

64

The most important addition to the sky model radiance predictions is the radiance from zodiacal light particles. These particles are concentrated along the ecliptic plane but extend throughout the sky. The data from Price (24) shows the ecliptic plane to be as bright as the galactic center (1.0E-11 Watts-cm^{-2}-um^{-1}-ster^{-1}), for an elongation angle of 75 degrees. The radiance falls off at higher ecliptic latitude, but is still seems brighter than the stellar background at most ecliptic latitudes (24).

The data from Hauser (11) shows the ecliptic plane to be as bright as the galactic center (1.6E-10 Watts-cm^{-2}-um^{-1}-ster^{-1}). The radiance falls off at higher ecliptic latitudes as does the Price data, but remains very intense at the ecliptic poles (4.6E-11 Watts-cm^{-2}-um^{-1}-ster^{-1}).

The Price data does not include values out to the ecliptic poles, but by extrapolating from the data available (table XII), the value is at least 1.0E-12 Watts-cm^{-1}-um^{-1}-ster^{-1}. This radiance is greater than the sky model prediction for galactic latitudes above 7 degrees. If the data from Hauser is used, the infrared sky at 12 microns is influenced mainly from zodiacal emission, and only the central portion of the galactic plane adds any contribution to background radiance. In fact, Hauser states in his data analysis "at 12, 25, and 60 microns, the zodiacal emission is evidently the dominant source at this resolution except near the galactic plane" (11:L15). While

65

the analysis of IRAS data by Hauser is only preliminary, it is suggestive that zodiacal emission at wavelengths around 11 microns is brighter than that estimated by Price (22).

It is difficult to plot radiance values for zodiacal light particles on an all sky map since the radiance varies with elongation angle from the Sun. As the earth revolves around the Sun, different stellar backgrounds pass through the entire range of elongation angles, 0 to 180 degrees. It is perhaps best to plot a median value of zodiacal emission based upon a constant elongation angle. While this will lead to excess radiance estimates at larger elongation angles, the data is not complete enough to be very precise, however. Accepting a constant elongation angle will lead to low estimates in the case of smaller elongation angles. This can be resolved by the fact that the sensor must always have an angular Sun avoidance zone. That is, a delicate sensor must not only avoid looking directly at the Sun, but must also avoid looking close to the Sun because of reflections from the optics and structure of the sensor. An elongation angle of 75 degrees is proposed since there is data from both Price and Hauser at this angle. This simplification will mean that ϵ larger elongation angles the sensor's range will be greater than predicted, but a smaller elongation angles, the sensor's range will be smaller.

The result of the above analysis indicates that the

66

infrared sky at wavelengths around 11 microns is divided into two regions: the galactic plane, dominated by sources within the central disk of the galaxy; and the remainder of the sky, dominated by emission from zodiacal light particles which are within in the solar system.

From the data from IRAS, AFGL, and zodiacal emission measurements, it appears that the infrared sky may have regions as intense at $1.6E-10$ Watts-cm^{-2}-um^{-1}-$ster^{-1}$ (11). The lowest radiance could be as low as $1.0E-12$ Watts-cm^{-2}-um^{-1}-$ster^{-1}$ (24), but the minimum could be as high as $4.6E-11$ Watts-cm^{-2}-um^{-1}-$ster^{-1}$ (11). With this data the maximum sensor range table (table VI) needs to be adjusted to show maximum ranges for irradiance levels between $1.0E-10$ and $1.0E-12$ Watts-cm^{-2}-um^{-1}-$ster^{-1}$. These ranges are shown in table XIV. Figure 14 shows the possible ranges graphically. The procedure to calculate the ranges is the same as in chapter IV.

Table XIV

Revised Maximum Ranges

Radiance Level Watts-cm^{-2}-um^{-1}-$ster^{-1}$	Range km
1.0E-11	2332
2.0E-11	1963
3.0E-11	1774
4.0E-11	1651
5.0E-11	1562
6.0E-11	1492
7.0E-11	1436
8.0E-11	1389
9.0E-11	1349
1.0E-10	1314
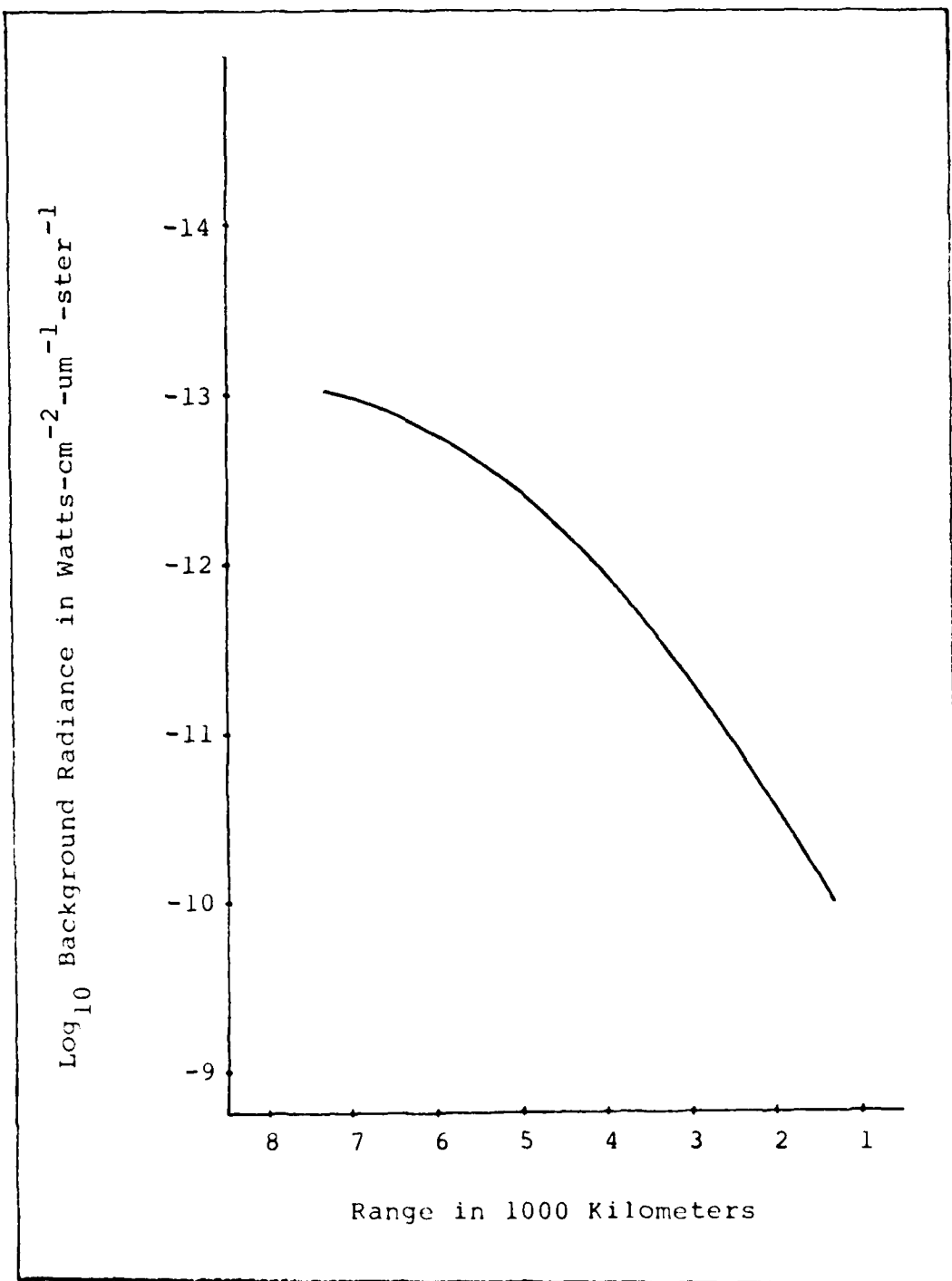
Figure 14.   Range versus Background Radiance

A rough plot of the minimum probable infrared background radiance around 11 microns is shown in Figure 15, plotted in galactic coordinates. This plot takes into account the estimates for both the galactic plane and zodiacal emission radiances. The maximum probable infrared background is about an order of magnitude above the values in Figure 15. There is a considerable difference between Figure 15 and the radiance contour chart in Figure 2.
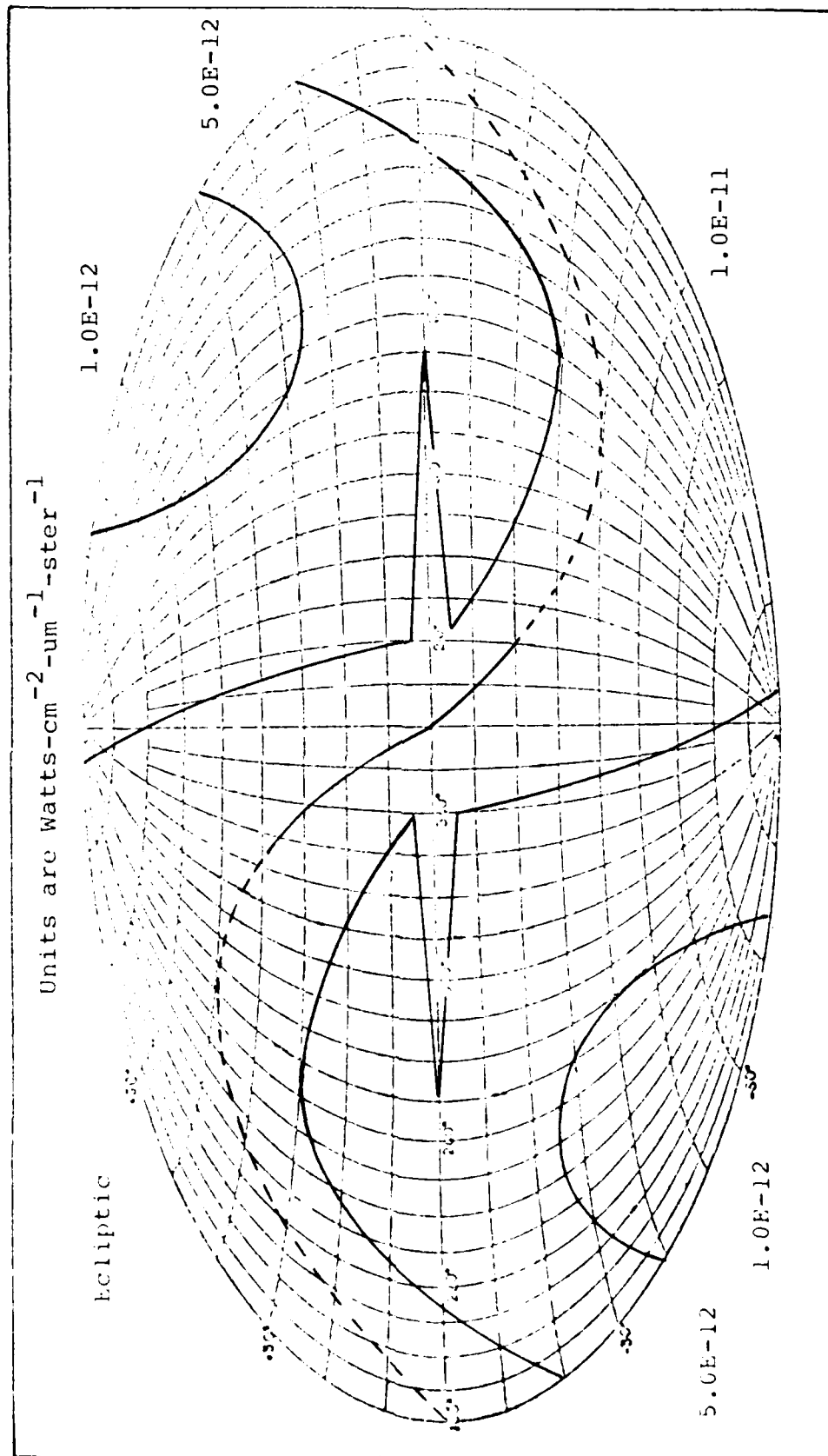
Figure 15. Revised Radiance Contour Map

70

VII. Conclusions and Recommendations

Several conclusions can be drawn from the analysis in this thesis. First, the data on the infrared sky at a wavelength of 11 microns is incomplete. Existing sky models are uncertain enough to dramatically affect satellite sensor performance. Secondly, more measurements of the zodiacal light are needed to resolve the uncertainties of the contribution of this source to the infrared background. When the entire IRAS data catalog becomes available and is analyzed, many of the data gaps can be filled.

There are several different factors that could change the maximum ranges that a sensor could be from a target and still detect it reliably. These include the size of the optics, the size of the target, the detector material, the number of detectors, and the signal processing algorithm. The example sensor in this thesis used a silicon-arsenide detector, much like the ones used on IRAS. Changing to a material like HgCdTe could improve the sensor's ability to detect fainter objects (3). Increasing the number of detectors to a two dimensional array such as a charge-coupled device and employing motion detection in the target signal processing could also improve the sensor's maximum range. Larger optics will increase system sensitivity as

71

well.

An area for further study could be an analysis of ASAT interception orbits to determine the precise path across the infrared background that a sensor would cover.

APPENDIX A

COORDINATE SYSTEMS

This thesis used three celestial coordinate systems, equatorial, ecliptic and galactic. Equatorial coordinates, as the name suggests, is referenced to the plane of the earth's equator. Ninety degrees from this plane is another plane in which the north and south celestial poles lie. Angles in the equatorial plane is measured in "right ascension," using hours, minutes and seconds, where 360 degrees are divided into 24 hours, 60 minutes per hour and 60 seconds per minute. Angles in the north-south plane is measured in "declination," using degrees, minutes and seconds (or decimal minutes). Declination is positive above the equator, and negative below the equator, just as latitude on the earth is measured.

Right ascension is measured from a zero point at the vernal equinox or as it is sometimes called "the first point of Aries." This point lies along a line of the intersection of the plane of the earth's equator with the plane of the earth's orbit around the sun. This point, the vernal equinox, γ, remains fixed with respect to the stars and forms the basis for this coordinate system. The earth's precession affects this point, but only to a slight degree over very very long time spans. The angle measured from this point to an object, measured in the

equatorial plane, in a easterly direction, is the object's

right ascension. In figure A-1, this is the angle between

and R. The angle from R to the object, measured in the R-

Z plane, is the objects declination. In figure A-2, the

object X's right ascension is the angle α and its

declination is the angle δ .

The plane containing the solar system is called the

ecliptic plane. When describing the position of objects in

the solar system its is often more convenient to define

their position with respect to the ecliptic. This

coordinate system uses ecliptic longitude, and ecliptic

latitude. The prime meridian for this ecliptic system is

the vernal equinox.

When the traces of the planes of the celestial equator

and ecliptic are drawn on the sky, their point of

intersection is at the vernal equinox. These two planes

are inclined at an angle of 23 degrees 26 minutes. This

angle is called the obliquity of the ecliptic ϵ .

Longitude is measured in degrees in an easterly direction

from the vernal equinox. Latitude is measure in degrees

above or below the ecliptic plane. In figure A-3, the

object X's ecliptic latitude is the angle β , its

ecliptic longitude is the angle λ .

When there is a need to represent the orientation of

stars or other objects in relation to the galaxy as a

whole, a galactic coordinate system is used. This system

74

uses latitude and longitude as the principal coordinates. While the galaxy is three dimensional, disk shaped, the galaxy is represented as a sphere with its central point at the Sun. The equator of this sphere runs through the center of the galactic disk. The "prime meridian" (fundamental line) of this coordinate system passes directly from the Sun through the center of the galaxy. Galactic longitude, "l", is the angle measured in a easterly direction, in the plane of galactic equator, between an object's position and the fundamental line.

The galactic equator divides the galaxy into two halves, one having positive latitude the other negative latitude. Galactic latitude "b" is the angle of an object from the galactic equator. See figure A-4.

The conversion of equatorial to galactic coordinate is accomplished by the following equation (6):

$$\text{Galactic Latitude}$$

$$"b" = \sin^{-1} \left[\sin \delta \sin 27°.4 + \cos \delta \cos(\alpha - 192.2°) + \cos \delta \sin 27°.4 \right]$$

Galactic Longitude

$$"l" = \tan^{-1} \left[\frac{\sin(d) - \sin(b)\sin(27.4)}{\cos(d)\sin(a-192.25)\cos(27.4)} \right] + 33$$

where:

a = the objects right ascension

d = the objects declination

The conversion of galactic to equatorial coordinates is accomplished by these equations:

Declination

$$"d" = \sin^{-1} \left[\cos(b)\cos(27.4)\sin(l-33) + \sin(b)\sin(27.4) \right]$$

Right Ascension

$$"a" = \tan^{-1} \left[\frac{\cos(b)\cos(l-33)}{\sin(b)\cos(27.4) - \cos(b)\sin(27.4)\sin(l-33)} \right] + 192.25$$

The conversion of equatorial coordinates to ecliptic coordinates is accomplished by the following (6),

$$\text{Ecliptic Longitude} = \tan^{-1} \left[\tan(a)\cos(\epsilon) + \frac{\tan(d)\sin(\epsilon)}{\cos(a)} \right]$$

Ecliptic Latitude = $\sin^{-1}\left[\sin(d)\cos(\epsilon) - \cos(d)\sin(\epsilon)\sin(a)\right]$

where

a = the object's right ascension,

d = the object's declination, and

ϵ = 23 degrees 26 minutes.

The conversion from ecliptic to equatorial coordinates is accomplished by the following (6),

Right Ascension = $\tan^{-1}\left[\tan(\lambda)\cos(\epsilon) - \dfrac{\tan(\beta)\sin(\epsilon)}{\cos(\lambda)}\right]$

Declination = $\sin^{-1}\left[\sin(\beta)\cos(\epsilon) + \cos(\beta)\sin(\epsilon)\sin(\lambda)\right]$

where

λ = the object's ecliptic longitude,

β = the object's ecliptic latitude, and

ϵ = 23 degrees 26 minutes.
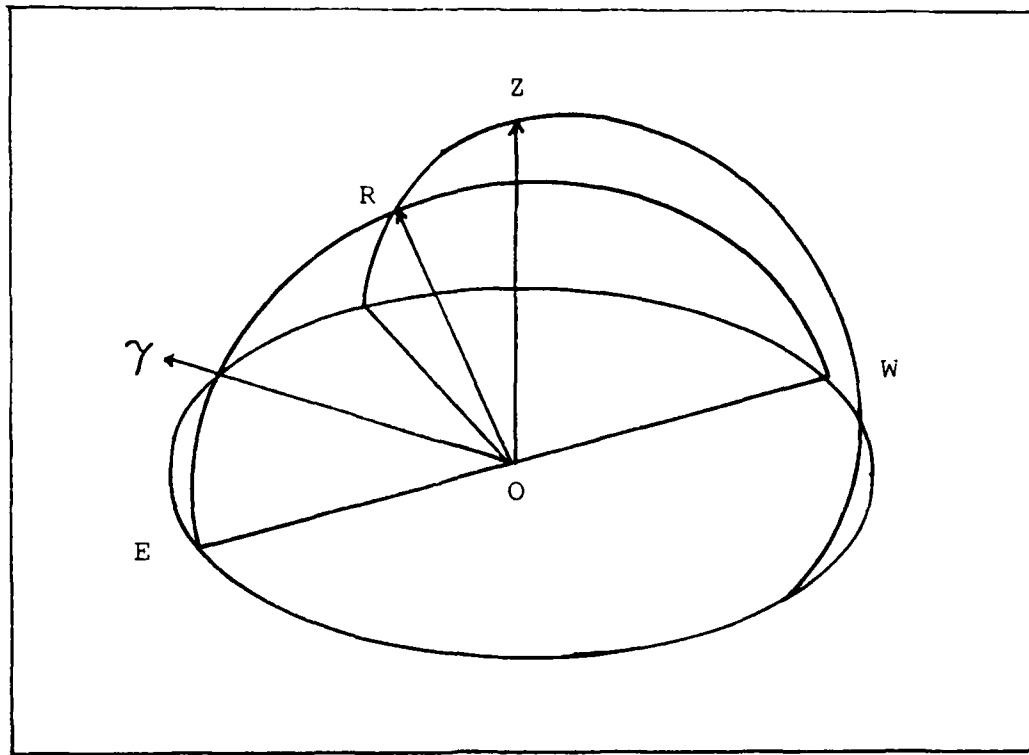
Figure A-1.   Equatorial Coordinates
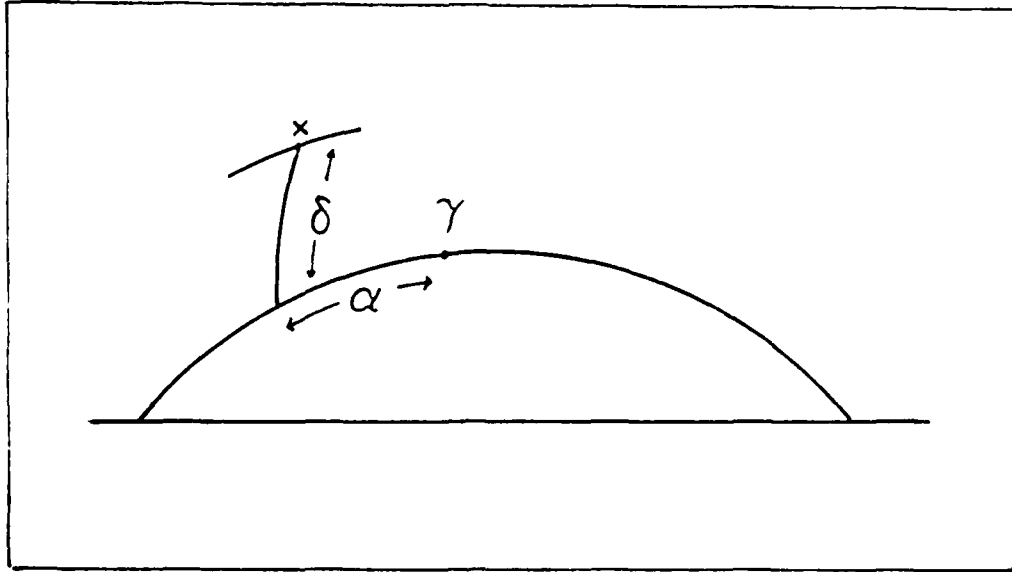
Figure A-2.   Right Ascension and Declination
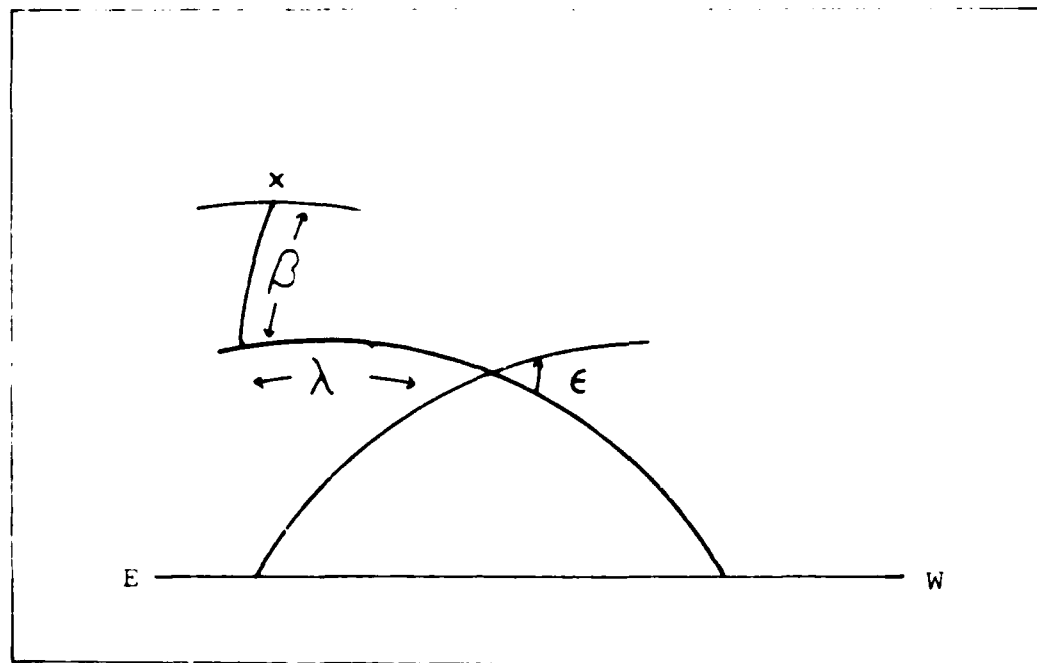
Figure A-3. Ecliptic Coordinates
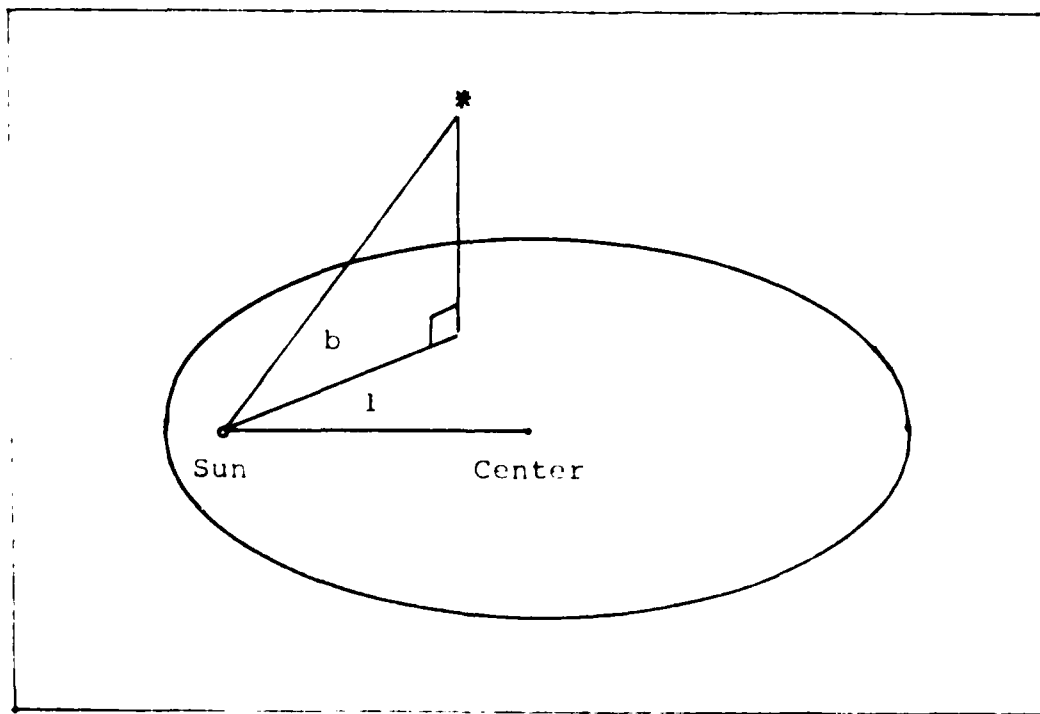
Figure A-4. Galactic Coordinates

79

Appendix B

Cataloged Observations

The following data is presented to two sections: the cataloged data from the AFGL catalog at 11 microns (25), and the discrete source data from the IRAS minisurvey at 12 microns (22). The AFGL data is for four areas, each 225 square degrees. The IRAS data covers 300 square degrees.

STAR DATA FOR AREA 1

Approximate Center

Galactic Latitude	0	Right Ascension 1900
Galactic Longitude	30	Declination	0

AFGL Number	Right Ascension	Declination	Magnitude
2210	183533	-0650.7	-6.10
2271	185050	+0110.4	-5.20
2390	192430	+1115.6	-4.20
2349	191240	-0708.3	-4.00
2381	192154	+1424.5	-3.60
2223	183953	-0221.1	-3.50
2206	183452	+1024.1	-3.40
2368	191736	-0806.1	-3.20
2402	192806	-0254.1	-3.20
2461	194724	-0743.4	-3.00
2177	182847	-0207.6	-2.90
2251	184502	-0203.0	-2.90
2334	190754	+0900.8	-2.70
2749	195456	-0200.4	-2.70
2139	182025	-1342.9	-2.60
2290	185604	+0638.3	-2.60
2350	191328	+0934.1	-2.50
2376	192009	+1358.5	-2.50
2227	183846	-0424.2	-2.40
2241	184115	+1353.1	-2.40
2324	190405	+0807.8	-2.40
2341	191102	+1047.5	-2.40
2147	182208	-1316.1	-2.30
2169	182630	-1055.2	-2.30
2178	182850	-0838.2	-2.30
2213	183559	+0845.6	-2.30
2310	190045	+0724.6	-2.30
2067	180404	-0941.8	-2.10
2113	181505	-1146.8	-2.10
2165	182459	-0351.5	-2.10
2190	183126	-0720.9	-2.10
2245	184323	-0242.6	-2.10
2291	185612	+1256.1	-2.10
2379	192044	+1410.0	-2.10
2119	181606	-1357.4	-2.00
2132	181829	-1304.3	-2.00
2304	185921	+0107.1	-2.00
2345	191158	+1104.9	-2.00

2088	180910	−0435.8	−1.90
2117	181543	−1346.4	−1.90
2154	182352	−0655.5	−1.90
2256	184637	−0658.4	−1.80
2272	185113	+0036.2	−1.80
2343	191122	+0003.5	−1.80
4250	193039	+1337.5	−1.80
2440	194114	+0338.3	−1.80
2136	181934	−1331.9	−1.70
2222	183731	−0236.0	−1.70
2223	183732	−0545.5	−1.70
2284	185347	+0751.1	−1.70
2378	192038	+1423.0	−1.70
4237	182242	−1318.0	−1.60
2316	190253	+0809.8	−1.60
2333	190733	+0920.1	−1.60
2374	191915	+0923.2	−1.60
2398	192738	+0249.6	−1.60
2152	182339	−1151.3	−1.50
2157	182422	−1242.0	−1.50
2205	183447	−0527.7	−1.50
2314	190139	−0546.4	−1.50
2108	181405	−1211.6	−1.40
2150	182307	+0543.8	−1.40
2203	183413	−0738.3	−1.40
2380	192055	+1447.7	−1.40
2423	193540	+1138.2	−1.40
4252	194107	−0004.5	−1.40
2057	180121	+0826.6	−1.30
2192	183137	−1133.3	−1.30
2199	183317	+0532.7	−1.30
2202	183351	−0723.4	−1.30
2243	184142	−0423.3	−1.30
2400	192737	−0056.6	−1.30
2065	180358	−0814.3	−1.20
2083	180738	−1033.5	−1.20
2127	181755	−1348.2	−1.20
2186	183037	−1410.8	−1.20

2193	183146	-0845.7	-1.20
2207	183504	-0622.3	-1.20
2266	184935	+1207.5	-1.20
2287	185515	+0322.9	-1.20
2288	185553	+0435.4	-1.20
2371	191813	+1349.8	-1.20
2161	182442	-1200.0	-1.10
2174	182818	-0945.2	-1.10
2185	183026	-0730.1	-1.10
2211	183539	-0532.5	-1.10
2259	184738	-0758.8	-1.10
2276	185216	+1035.3	-1.10
2392	192455	+0656.9	-1.10
2453	194357	+1030.7	-1.10
4253	194526	+0921.9	-1.10
2118	181542	-0655.0	-1.00
2168	182615	-1134.7	-1.00
2188	183053	-0910.7	-1.00
2194	183149	-0759.3	-1.00
2229	183928	-0505.2	-1.00
2070	180443	+0633.4	-.90
2153	182352	-1226.8	-.90
2164	182459	-0842.6	-.90
2166	182511	-1304.1	-.90
2248	184426	-0447.8	-.90
2239	184049	+1221.7	-.80
2326	190433	+0705.0	-.80
2329	190540	+0612.6	-.80
2195	183202	-0836.1	-.70
2142	182128	+0335.7	-.60
2282	185341	-1036.3	-.60
2359	191509	+1150.9	-.60
2123	181705	-1220.6	-.50
2204	183444	-0243.1	-.50
2254	184539	-0206.6	-.50
2179	182855	-1000.3	-.40

STAR DATA FOR AREA 2

Approximate Center

Galactic	Latitude	5	Right Ascension	0700
Galactic	Longitude	210	Declination	0

AFGL Number	Right Ascension	Declination	Magnitude
0877	060519	-0623.3	-2.70
0915	061735	-1036.0	-2.70
1028	065007	+0827.9	-2.60
0865	060118	+0725.4	-2.40
0971	063419	+0326.4	-2.20
1059	070122	-1128.7	-1.80
1074	070527	-1039.3	-1.80
0921	061921	-0351.0	-1.60
0999	064018	-1423.7	-1.60
1135	072808	-0938.7	-1.60
1138	073001	+0826.3	-1.60
0968	063319	+0901.9	-1.50
1060	070208	-0853.1	-1.40
0918	061813	+1135.0	-1.30
0935	062302	-0929.1	-1.30
0977	063456	-0121.3	-1.30
1017	064704	+0301.4	-1.30
1062	070240	-1457.1	-1.30
1075	070543	-1150.6	-1.30
0933	062239	-0906.5	-1.20
1038	065304	+0624.9	-1.20
1070	070431	-0729.5	-1.20
0940	062359	+0902.9	-1.10
0989	063826	+0932.3	-1.10
1215	075827	-1243.1	-.90
0837	060355	-0543.3	-.80
1022	064921	+0449.1	-.80
0934	062243	+1444.1	-.70
1199	074843	-0232.1	-.70
0902	061131	+1352.2	-.60
0967	063306	+1415.1	-.50
0961	063154	+0416.6	-.40

STAR DATA FOR AREA 3

Approximate Center

Galactic Latitude	60	Right Ascension	1200
Galactic Longitude	270	Declination	0

AFGL Number	Right Ascension	Declination	Magnitude
1594	125956	+0525.9	-2.50
1554	122748	+0442.8	-2.20
1579	124441	+0424.8	-1.70
1586	125254	+0338.6	-1.50
1575	124241	-0614.9	-1.40
1535	120443	-0629.0	-1.30
1566	123546	+0206.2	-1.20
1583	125139	-0915.8	-1.10
1495	112913	-1205.3	-.90
1549	122238	+0101.4	-.90
1458	110453	-1111.7	-.80
1516	114835	-1056.2	-.80
4156	123251	+0618.6	-.50
1487	112320	+0930.5	-.30

STAR DATA FOR AREA 4

Approximate center

Galactic Latitude -60°   Right Ascension

Galactic Longitude 90°   Declination

AFGL Number	Right Ascension	Declination	Magnitude
3099	232545	+1038.4	
0085	003257	-1146.0	
0066	002426	-0654.9	-.4
3023	230406	+1015.5	-.4
3031	230658	+0823.9	
3059	231415	+1018.3	
3147	234348	+0311.3	
3197	235928	-0616.4	-1.
3083	232006	-1107.4	-.70
3058	231417	-0801.3	-.50

IRAS Number	Right Ascension	Declination	Janskys
0347+275p10	034725	+2731.1	4.6
0349+268p10	034910	+2649.6	1.2
0350+253p10	035004	+2523.8	1.8
0351+231p10	035145	+2310.4	5.3
0354+243p10	035427	+2419.1	2.7
0355+237p10	035538	+2343.0	1.6
0357+199p10	035751	+1955.8	0.2
0358+200p10	035812	+2003.0	1.0
0358+183p10	035817	+1819.8	1.0
0359+209p10	035943	+2055.7	2.0
0359+165p10	035955	+1632.3	4.4
0400+127p10	040045	+1245.7	1.1
0401+181p10	040111	+1810.9	7.6
0401+239p10	040122	+2358.2	4.1
0401+190p10	040124	+1904.8	4.7
0401+123p10	040132	+1222.3	9.6
0401+219p10	040144	+2156.8	7.3
0402+212p10	040219	+2114.3	0.2
0402+219p10	040222	+2155.4	0.8
0402+218p10	040223	+2152.5	0.8
0402+156p10	040238	+1541.8	1.1
0403+245p10	040304	+2435.9	3.3
0404+231p10	040406	+2310.9	1.8
0405+214p10	040415	+2125.3	4.7
0405+099p10	040558	+0958.1	7.9
0406+194p10	040615	+1928.7	3.2
0406+085p10	040630	+0831.1	0.4
0407+111p10	040717	+1107.5	0.9
0408+165p10	040812	+1631.1	0.6
0408+127p10	040827	+1245.7	1.1
0408+068p10	040831	+0653.4	1.2
0408+081p10	040837	+0809.6	4.2
0409+171p10	040939	+1709.0	1.6
0409+054p10	040943	+0525.2	0.7
0409+145p10	040953	+1430.6	1.3
0410+049p10	041005	+0454.3	0.9
0410+132p10	041026	+1317.6	0.4
0410+037p10	041046	+0346.0	3.6
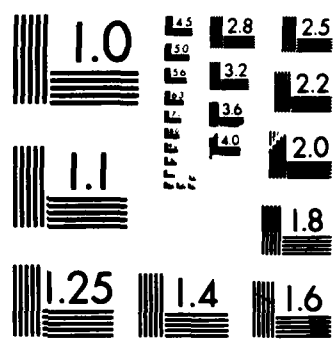
MICROCOPY RESOLUTION TEST CHART

NATIONAL BUREAU OF STANDARDS-1963-A

0410+100p10	041051	+1005.1	1.3
0411+134p10	041101	+1329.7	0.9
0411+126p10	041103	+1237.7	1.6
0411+144p10	041103	+1425.4	3.7
0411+021p10	041150	+0206.6	1.3
0413+061p10	041300	+0606.4	3.6
0413+122p10	041348	+1217.6	0.2
0414+001p10	041410	+0009.0	0.3
0414+103p10	041429	+1020.0	0.4
0414+023p10	041442	+0218.7	0.4
0415+014p10	041508	+0126.4	0.2
0417+000p10	041731	+0005.9	0.3
0417-027p10	041745	-0244.8	8.7
0418+060p10	041802	+0600.8	1.7
0418+010p10	041830	+0104.6	1.4
0418-032p10	041840	-0317.4	1.9
0418-019p10	041841	-0155.6	3.5
0418-002p10	041853	-0012.9	3.7
0419+037p10	041909	+0346.9	5.2
0419+039p10	041918	+0355.8	0.3
0420-056p10	042007	-0537.0	7.6
0421-070p10	042147	-0705.3	1.1
0422+022p10	042248	+0214.5	2.8
0423-006p10	042354	-0037.3	2.9
0424-093p10	042404	-0922.4	0.9
0424-062p10	042444	-0614.1	0.3
0424-021p10	042454	-0207.6	3.3
0427-126p10	042727	-1236.7	0.2
0429-046p10	042911	-0441.7	1.0
0430-126p10	043047	-1238.8	1.1
0431-108p10	043100	-1053.4	3.9
0432-143p10	043232	-1419.3	1.2
0435-177p10	043526	-1746.8	1.9
0437-170p10	043729	-1703.6	2.1
0428-177p10	043812	-1746.7	1.8
0438-197p10	043815	-1946.0	72.0
0440-205p10	044005	-2031.7	0.3
0442-219p10	044210	-2158.3	0.2

0453-299p10	045354	-2957.7	0.3
1638-136p10	163812	-1341.0	1.4
1640-141p10	164038	-1406.4	24.0
1641-094p10	164126	-0927.6	5.8
1641-139p10	164153	-1359.3	8.3
1642-123p10	164217	-1223.9	0.8
1643-089p10	164302	-0856.7	0.4
1643-079p10	164335	-0758.8	3.3
1643-103p10	164344	-1020.7	1.5
1643-115p10	164353	-1133.6	130.0
1644-095p10	164414	-0930.0	0.5
1646-113p10	164612	-1119.2	2.2
1646-067p10	164620	-0642.2	0.4
1646-050p10	164627	-0503.4	1.0
1646-088p10	164659	-0850.4	1.8
1647-106p10	164702	-1041.8	2.0
1647-113p10	164737	-1122.9	1.8
1648-061p10	164837	-0609.7	5.1
1648-023p10	164847	-0222.2	0.2
1648-030p10	164855	-0300.8	0.4
1649-088p10	164910	-0849.4	1.2
1649-084p10	164956	-0824.8	0.3
1649-053p10	164956	-0522.5	3.2
1649-046p10	164957	-0437.5	8.3
1650-048p10	165028	-0450.8	2.4
1650-769p10	165049	-7654.7	0.2
1650-101p10	165058	-1010.1	2.3
1651-075p10	165126	-0733.3	0.4
1651-066p10	165137	-0637.9	3.9
1651-098p10	165137	-0948.5	0.5
1651-074p10	165149	-0728.8	11.0
1651-060p10	165155	-0604.4	3.8
1652-093p10	160215	-0923.7	2.2
1652-082p10	165226	-0817.3	1.2
1652-065p10	165227	-0634.3	1.4
1652-082p10	165246	-0815.2	1.1
1652-034p10	165256	-0329.7	1.7
1653-040p10	165320	-0401.9	1.2

1653-011p10	165324	-0110.3	0.2
1653-020p10	165332	-0201.5	1.5
1654-013p10	165406	-0121.2	0.4
1654+029p10	165443	+0257.6	0.4
1654+000p10	165452	+0005.5	3.2
1655-026p10	165514	-0241.2	13.0
1657+050p10	165724	+0503.4	2.4
1657+050p10	165755	+0505.9	3.9
1657+045p10	165759	+0433.3	1.2
1658+022p10	165816	+0212.6	4.5
1658+069p10	165843	+0655.8	0.3
1658+074p10	165853	+0730.0	1.0
1658+053p10	165855	+0521.3	0.3
1659+041p10	165901	+0410.5	1.0
1659+066p10	165920	+0640.9	3.3
1659+022p10	165936	+0216.9	1.0
1700+062p10	170024	+0612.2	2.1
1700+003p10	170029	+0019.4	1.2
1700+048p10	170033	+0449.0	2.7
1700-757p10	170038	-7546.8	1.1
1702+080p10	170244	+0803.4	1.0
1703+038p10	170305	+0350.1	7.0
1703+051p10	170330	+0506.2	1.8
1703+086p10	170343	+0841.4	2.0
1703+097p10	170347	+0948.0	2.9
1703+104p10	170358	+1026.3	0.4
1703+036p10	170359	+0341.9	0.8
1705+054p10	170553	+0527.7	1.4
1706+084p10	170616	+0829.6	1.3
1706+084p10	170631	+0826.1	2.4
1710+106p10	171006	+1038.6	18.0
1710+116p10	171016	+1139.2	1.0
1710+117p10	171019	+1142.9	1.2
1710+111p10	171034	+1107.2	1.1
1712+111p10	171219	+1107.5	66.0
1712+144p10	171222	+1426.7	1700.0
1712+154p10	171245	+1527.1	1.0
1714+131p10	171452	+1311.3	1.5

1715-769p10	171516	-7656.9	1.6
1715+171p10	171545	+1710.6	1.2
1715+133p10	171549	+1323.5	1.1
1716+163p10	171624	+1620.1	0.7
1716+152p10	171644	+1517.6	1.7
1716+147p10	171646	+1447.7	1.3
1717+164p10	171702	+1626.9	1.1
1717+181p10	171723	+1810.1	2.8
1718+181p10	171806	+1806.3	20.0
1719+186p10	171914	+1836.2	3.2
1719+167p10	171919	+1646.7	8.4
1720+171p10	172018	+1710.5	1.1
1721+211p10	172151	+2111.0	0.4
1723+199p10	172305	+1957.8	1.4
1723+195p10	172332	+1935.9	1.4
1723+202p10	172346	+2014.7	2.8
1724+221p10	172417	+2209.0	0.9
1728+240p10	172835	+2404.7	2.0
1729+236p10	172914	+2339.5	1.0
1730+254p10	173051	+2527.2	1.7
1731+236p10	173116	+2337.3	2.0
1732+264p10	173239	+2625.2	1.0
1733+243p10	173307	+2422.8	1.9
1734-794p10	173430	-7927.1	0.9
1735+254p10	173538	+2524.0	2.9
1738-792p10	173852	-7916.0	4.2
1823-823p10	182318	-8219.9	1.7

Appendix C

Infrared Flux Units

There are three flux units used in this thesis: Watts-cm^{-2}-um^{-1}, magnitudes, and Janskys. Magnitude is a system that originated with measuring stellar brightness at visible wavelengths. The flux unit Jansky is used for measurements of astronomical sources in the infrared. All comparisons in this thesis is done in Watts-cm^{-2}-um^{-1}.

The stellar magnitude system was developed by Pogson in 1856 (1). The basis of this scale is the definition that a star of magnitude m is 2.512 (or the 5th root of 100) times as bright as a star of magnitude m+1. That is, the higher the magnitude of the fainter the star. For negative magnitudes, a more negative magnitude is brighter than a less negative magnitude. If the light flux from two stars is L1 and L2, the magnitude (abbreviated m) difference between them is:

$$m1 - m2 = 2.5 \log\left(\frac{L2}{L1}\right)$$

Table C-I shows magnitude differences and approximate light ratios. For magnitudes listed in Appendix B, the reference magnitude of 0.0 is set at 8.3E-17 Watts-cm^{-2}-um^{-1} (27).

The Jansky is a flux unit defined as 1.0E-26 Watts-meter^{-2}-Hertz^{-1} (16). This unit is wavelength dependent. The Jansky is used as a flux unit for the IRAS data in Appendix B. The wavelength for the IRAS data presented is

12 microns. Converting the Jansky to Watts-cm^{-2}-um^{-1} for 12 microns yields as conversion factor of 2.08E-18. That is, for 12 micron observations, multiplying the number of Janskys by 2.08E-18 will yield the object's irradiance in Watts-cm^{-2}-um^{-1}.

TABLE C-I

Magnitude Differences and Light Ratios

Magnitude Difference	Light Ratio
0.0	1:1
0.5	1.6:1
0.75	2:1
1.0	2.5:1
1.5	4:1
2.0	6.3:1
2.5	10:1
3.0	16:1
4.0	40:1
5.0	100:1
6.0	251:1
10.0	10000:1

Appendix D

Walker Sky Model Derivation

This appendix shows the derivation of the formulae for the Walker Sky Model. The model predicts how many infrared sources can be seen in a 1 by 1 degree area of the sky in the direction defined by the galactic latitude b and longitude l.

The number of sources seen along any line-of-sight will be a function of the density of the sources. The Walker Model assumes there are three classes of objects, dwarf stars, giant stars, and supergiant stars. The model assumes that density of stars of type i at any particular point (r_i, b) is given by

$$n_i \left(\frac{R_c^2}{R_c^2 + R_i^2} \right) \exp\left[-r_i^2 \left(\frac{\sin b}{\sigma_i^2} \right)^2 \right]$$

where

n_i = the mean space density along the galactic plane in numbers/cm^3,

r_i = the distance from the sun,

R_c = the radius of the galactic nucleus,

R_i = the distance in the galactic plane from the galactic center to some arbitrary point

94

defined by r_i (see figure 1),

b = the galactic latitude

σ_i = the standard deviation of the galactic distribution of a particular class of objects in terms of perpendicular distance from the galactic plane.

The number of objects seen in a 1 by 1 degree area will be determined by the number of objects in the volume formed by projecting the 1 by 1 degree area to maximum distance Rmax. This is shown in figure D-1.

The differential volume element is

$$\Delta V = \Delta r \left(\Delta b r \right)^2$$

where

r = the *distance from* the sun to the volume element,

Δr = the length of the volume element,

Δb = the angular width of the volume element.

The total number of objects in the volume is the density of the objects times the total volume,

$$N = \int_0^{R_{max}} r_i^2 \, n_i \, F \left(\Delta b \right)^2 dr_i$$

where

Rmax = the maximum distance that objects can still be detected by a sensor before they become too faint,

$$F = \left[\left(\frac{R_c^2}{R_c^2 + R_i^2} \right) exp\left(-r_i^2 \left(\frac{sin\,b}{\sigma_i^2} \right)^2 \right) \right]$$

The distance Rmax is dependent upon the irradiance of the sources and cannot be measured directly. However, a minimum detectable radiance can be defined, and a change of integration variable is in order. Since the radiance

$$E_\lambda = \frac{I_{\lambda,i}}{r_i^2} \qquad and \quad r_i = \left(\frac{I_{\lambda,i}}{E_\lambda} \right)^{1/2},$$

then $d\,r_i = \dfrac{I_{\lambda,i}^{1/2}}{-2\,E_\lambda^{3/2}}\, d E_\lambda$

where $I_{\lambda,i}$ = the mean spectral intensity of the ith class of objects in watts/ster.

Then the limits of integration become

$$r_i = 0 \longrightarrow E_{\lambda,i} = \infty$$

$$r_i = R_{Max} \longrightarrow E_{\lambda,i} = \left(E_{\lambda_i} \right)_{min}$$

Substituting these terms for r_i^2 and dr_i leads to

$$N = \int_{E_{\lambda MIN}}^{\infty} n_i F \frac{I_{\lambda,i}}{E_\lambda} \left(\frac{I_{\lambda,i}^{1/2}}{E_\lambda^{3/2}}\right) dE_\lambda$$

Since $I_{\lambda,i}$ and n_i are constants,

$$N = I_{\lambda,i}^{3/2} n_i \int_{E_{\lambda MIN}}^{\infty} F E_\lambda^{-5/2} dE_\lambda$$

The total number of sources is the sum of all classes,

$$N = \sum_{i=1}^{M} I_{\lambda,i}^{3/2} n_i \int_{E_{\lambda MIN}}^{\infty} F E_\lambda^{-5/2} dE_\lambda$$

Substituting for F gives

$$N = \sum_{i=1}^{M} I_{\lambda,i}^{3/2} n_i \int_{E_{\lambda MIN}}^{\infty} E_\lambda^{-5/2} \left(\frac{R_c^2}{R_c^2 + R_i^2}\right) exp\left(-r_i^2 \left(\frac{sin b}{\sigma_i^2}\right)^2\right) dE_\lambda$$

97

Since $r_i^2 = I_{\lambda,i}/E_\lambda$ and allowing $k = 1.52E-4$ to convert from number/ster to number/deg^2, Walker's formula is arrived at,

$$N = k \sum_{i=1}^{m} I_{\lambda,i}^{3/2} \; n_i \int_{E_{\lambda min}}^{\infty} E_\lambda^{-5/2} \left(\frac{R_c^2}{R_c^2 + R_i^2} \right) \exp\left(-\frac{I_{\lambda,i}}{E_\lambda} \left(\frac{\sin b}{\sigma_i^2} \right)^2 \right) d E_\lambda$$
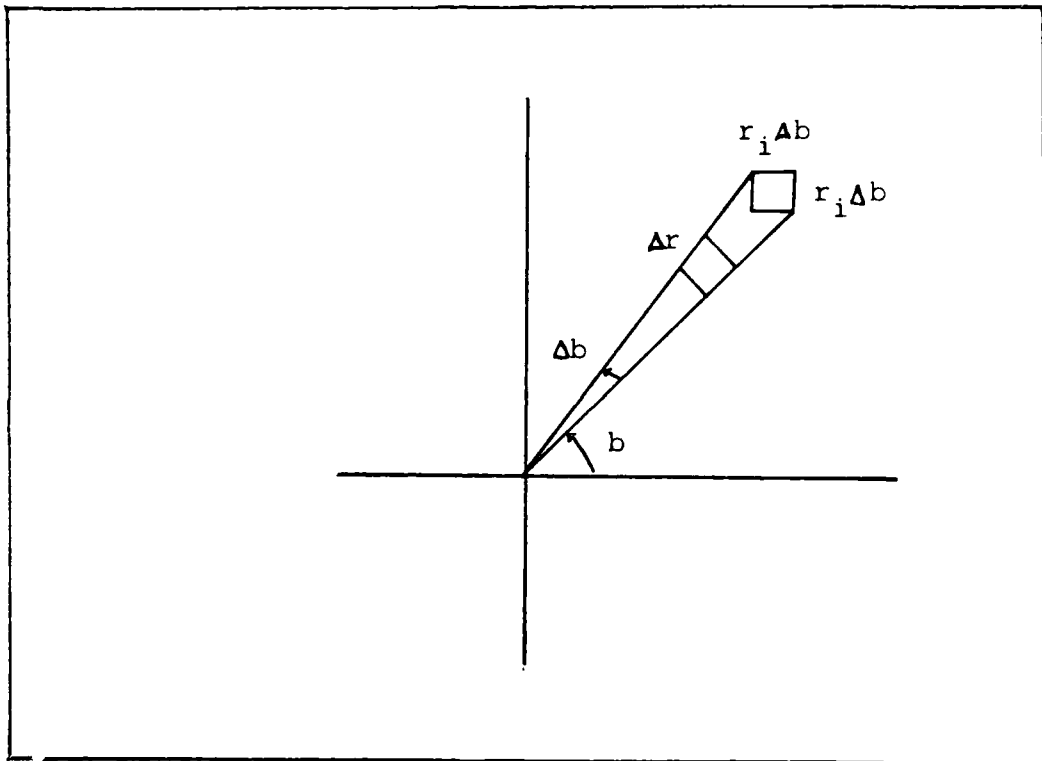

Figure D-1. Volume Element

BIBLIOGRAPHY

1.   Abell, George, Exploration of the Universe, Holt, Rinehart, and Winston, New York, 1969, pp 253 and 512.

2.   Beatty, J. Kelly, "A Telescope in a Bottle", Sky and Telescope, vol. 67, no. 2, February 1984, p. 124.

3.   Chapman, R.A., and M.A. Kinch, "HgCdTe Charge-Coupled Devices," AIAA/NASA Conference on "Smart" Sensors, Number 14-16, Hampton, Virginia, 1978, page 1.

4.   Chartrand, Mark, "ASAT ABC's", Space world, vol. T-4-232, April 1983, pp 7-10.

5.   David, L. "The U.S. ANTIs Up (Miniature Homing Vehicle)" Space World, vol. U-4-244, April 1984, p 12.

6.   Duffet-Smith, Peter, Practical Astronomy With Your Calculator, Cambridge University Press, New York, 1979, pp. 17-35.

7.   Garwin, Richard L. and John Pike, "Space Weapons, History and Current Debate," Bulletin of the Atomic Scientists, vol. 4, no. 5, May 1984, p. 5S.

8.   Gezari, Daniel Y., Marion Schmitz, and Jaylee M. Mead, "Catalog of Infrared Observations," NASA Reference Publication 1118, May 1984.

9.   Grasdalen, Gary L., R. D. Gehrz, J. A. Hackwell, M. Castelez, and C. Gullixson, "The Stellar Component of the AFGL Infrared Sky Survey", The Astrophysical Journal Supplement Series, vol. 53, October 1983, pp 413-457.

10. Greenbaum, M. Computer Implementation of the Walker Star Model, Research Note N-1/364-3-64, Riverside Research Institute, New York, 1977.

11. Hauser, M. G., et al, "IRAS Observations of the Diffuse Infrared Background", The Astrophysical Journal Letters, vol. 278, 1 March 1984, pp L15-L18.

12. Lange, James J. Lecture materials distributed in PHY 521, Space Surveillance, and PHY 621, Electro-Optical Systems. School of Engineering, Air Force Institute of Technology (AU), Wright-Patterson AFB OH, October 1983.

13. Leinert, C., M. Hanner, and E. Pitz, "On the Spatial Distribution of Interplanetary Dust Near 1 AU," _Astronomy and Astrophysics_, vol. 63, 1978, pp. 183-187.

14. Limperis, Thomas and Joseph Mudar, "Detectors," _The Infrared Handbook_, William L. Wolfe, Editor, Environmental Research Institute of Michigan, Office of Naval Research, Department of the Navy, Washington, D.C., 1978, pp. 11-1 to 11-84.

15. _LWIR Technology Assessment Study_, Air Force Space and Missile Systems Report SAMSO-TR-75-218, vol 5., 11 August 1975 (SECRET).

16. Low, F. J., and G. H. Rieke, "The Instrumentation and Techniques of Infrared Photometry," _Methods of Experimental Physics_, vol. 12 Academic Press, New York, 1979, pp. 451-460.

17. Lowndes, Jay C., "Satcom Filings Crowd Orbital Capacity," _Aviation Week and Space Technology_, vol. 118, no. 11, pp. 104-105.

18. Lyons, Jack K. and John F. Heintz, "The Satellite Infrared Program (SIRE)", _The Sixth Strategic Space Symposium_, 14-16 March 1978. (SECRET)

19. McCreight, C. R. and H. Lum, "Integrated Detector Array Preprocessing For Infrared Astronomical Applications", _Remote Sensing of Earth from Space: Role of Smart Sensors_, American Institute of Aeronautics and Astronautics, New York, 1979 pp 455-468.

20. McCreight, C. R., R. G. Walker, and F. E. Witteborn, "Infrared Astronomy Satellite (IRAS) and Shuttle Infrared Telescope Facility: Implications of Scientific Objectives on Focal Plane Sensitivity Requirements," _Society of Photo-Optical Instrumentation Engineers_, Volume 132, 1978, pp 66-70.

21. Murdock, T. L., _The Contribution of Asteroids to the Infrared Astronomical Sky Survey_, AFCRL-TR-73-0154, 9 March 1973.

22. Neugebauer, G. and H. Habing, "IRAS Circular No. 10," _Astronomy and Astrophysics_, Volume 132, 1984 ,pp C1-C4.

23. Price, Stephen D., "Data Bases for Infrared Celestial Backgrounds," paper from the _Eighth Strategic Space Symposium_, 1980, pp. 2-1 to 2-17.

24.   Price, S. D., T. L. Murdock, and L. P. Marcotte, "Infrared Observations of the Zodiacal Dust Cloud", The Astronomical Journal, vol. 85, no. 6, June 1980, pp 765-771.

25.   Price, Stephan D., "Infrared Mapping of the Galactic Plane. I. Low-Resolution Maps Between 0 and 320 Longitude," The Astronomical Journal, vol. 86, no. 2, 1981 pp. 193-205.

26.   Price, Stephan D., Leonard P. Marcotte, and Thomas L. Murdock, "Infrared Mapping of the Galactic Plane II, Medium-Resolution Maps of the Cygnus X Region," The Astronomical Journal, vol. 87, no. 1, 1982, pp 131-139.

27.   Price, Stephen D., and Russel G. Walker, The AFGL Four Color Infrared Sky Survey: Catalog of Observations at 4.2, 11.0, 19.8, and 27.4 microns, AFGL-TR-0208, Air Force Geophysics Laboratory, Hanscom AFB Mass., 17 September 1976.

28.   Robinson, Leif J., "The Frigid World of IRAS", Sky and Telescope, vol. 67, no. 1, January 1984, pp 4-8.

29.   Rowan-Robinson, M., P. E. Clegg, et al, "The IRAS Minisurvey," The Astrophysical Journal, vol. 278, March 1984, pp. L7-L10.

30.   Ruffatto, Donald, "LWIR Satellite Signature Program" Briefing for AMOS Program Review, ARPA Maui Optical Station, Maui, Hawaii, 15 March 1982.

31.   Soifer, Baruch T., J. R. Houck, and Martin Harwit, "Rocket-Infrared Observations of the Interplanetary Medium," The Astrophysical Journal, vol. 168, 1971, pp. L73-L78.

33.   Smith, Bruce A., "Air Force Cancels Infrared Spacecraft", Aviation Week and Space Technology, vol. 110, no. 23, 4 June 1979, page 22.

34.   The USAF Space Surveillance Program Architecture, vol II, Technical Supplement, Air Force Space Division Report, SD-82-29, September 30, 1981. (SECRET)

35.   "USAF Reviews Surveillance System Technology," Aviation Week and Space Technology, vol. 120, no. 10, 5 March 1984, page 62.

36.   Walker, Russel G. "The Celestial Background in the Spectral Range from 4.0 to 30.0 Microns," The Infrared Handbook, William L. Wolfe editor, Office of Naval Research, Department of the Navy, Washington, D.C., 1978, pp 3-27 to 3-34.

37.   Walker, R. G. and H. H. Aumann, "Infrared Astronomical Satellite," Optical Engineering, vol. 16, no. 6, November 1977, pp. 537-543.

VITA

Captain Jeffery G. Horne was born 23 May 1953 in Ventura, California. He graduated from high school in Ventura, California in 1971 and attended the University of California, Los Angeles from which he received a Bachelor of Arts degree in Astronomy in June 1975. Upon graduation, he received a commission in the USAF through the ROTC program. Called to active duty in July 1976, he served as a Space Systems Director at the 2nd Communications Squadron, Buckley ANGB, Colorado through September 1978. He was transferred to the 16th Surveillance Squadron, Shemya AB Alaska, and served as a Space Surveillance Officer through September 1979. He was transferred to the Air Force Satellite Control Facility, Sunnyvale, California and obtained a Master of Science degree in Systems Management from the University of Southern California while serving as a Space Shuttle Operations Team Chief until entering the School of Engineering, Air Force Institute of Technology in June 1983.

Permanent Address: 171 Lakewood Avenue
Ventura, CA 93004

REPORT DOCUMENTATION PAGE

A182594

1a. REPORT SECURITY CLASSIFICATION UNCLASSIFIED		1b. RESTRICTIVE MARKINGS			
2a. SECURITY CLASSIFICATION AUTHORITY		3. DISTRIBUTION/AVAILABILITY OF REPORT Approved for public release; distribution unlimited			
2b. DECLASSIFICATION/DOWNGRADING SCHEDULE					
4. PERFORMING ORGANIZATION REPORT NUMBER(S)		5. MONITORING ORGANIZATION REPORT NUMBER(S)			
6a. NAME OF PERFORMING ORGANIZATION AFIT/GSO/PH/84D-4	6b. OFFICE SYMBOL (If applicable)	7a. NAME OF MONITORING ORGANIZATION			
6c. ADDRESS (City, State and ZIP Code) Air Force Institute of Technology Wright Patterson AFB, Ohio 45433		7b. ADDRESS (City, State and ZIP Code)			
8a. NAME OF FUNDING/SPONSORING ORGANIZATION	8b. OFFICE SYMBOL (If applicable)	9. PROCUREMENT INSTRUMENT IDENTIFICATION NUMBER			
8c. ADDRESS (City, State and ZIP Code)		10. SOURCE OF FUNDING NOS.			

10. SOURCE OF FUNDING NOS.			
PROGRAM ELEMENT NO.	PROJECT NO.	TASK NO.	WORK UNIT NO.

11. TITLE (Include Security Classification) see box 19

12. PERSONAL AUTHOR(S)
Jeffery G. Horne, B.A.,M.S., Capt,USAF

13a. TYPE OF REPORT MS Thesis	13b. TIME COVERED FROM _____ TO _____	14. DATE OF REPORT (Yr., Mo., Day) 1984 December	15. PAGE COUNT 111

16. SUPPLEMENTARY NOTATION

17. COSATI CODES			18. SUBJECT TERMS (Continue on reverse if necessary and identify by block number)
FIELD	GROUP	SUB. GR.	Antisatellite Defense Systems, Infrared Detectors, Infrared Stars, Interplanetary Space, Space Surveillance
03	01		
22/17	02 05		

19. ABSTRACT (Continue on reverse if necessary and identify by block number)

Title: SENSOR DESIGN OF GEOSYNCHRONOUS
         ANTISATELLITE VEHICLES

Thesis Advisor: James J. Lange, Major, USAF

20. DISTRIBUTION/AVAILABILITY OF ABSTRACT UNCLASSIFIED/UNLIMITED XX SAME AS RPT. ☐ DTIC USERS ☐	21. ABSTRACT SECURITY CLASSIFICATION UNCLASSIFIED	
22a. NAME OF RESPONSIBLE INDIVIDUAL James J. Lange, Major, USAF	22b. TELEPHONE NUMBER (Include Area Code) 513-255-4498	22c. OFFICE SYMBOL AFIT/ENP

DD FORM 1473, 83 APR   EDITION OF 1 JAN 73 IS OBSOLETE

The maximum distance from which a possible
antisatellite sensor can reliably detect its target was
investigated based upon the celestial background radiation
at a wavelength of 11 microns. A sensor design was
postulated and assessed with various background conditions.
The analysis was first conducted using the Walker Sky
Model to estimate the amount of infrared background
radiance from stellar sources. Then this estimate was
compared with cataloged observations from the Air Force
Geophysics Lab catalog and preliminary data from the
Infrared Astronomical Telescope. In addition, the amount
of infrared radiation from asteroids and zodiacal light
particles was also considered.
The results of the analysis indicates that for a
sensor using a single detector, a spinning reticle, and
optics 20 centimeters in diameter, the maximum range that
a one square meter target can be detected reliably is between
1300 and 2300 kilometers. However, more investigations
into the infrared stellar and zodiacal light background are
needed as the currently available data is incomplete.

END
8-87
DTIC